Past, present, and future variations of extreme precipitation in Denmark

Technical report

Gregersen, Ida Bülow; Sunyer Pinya, Maria Antonia; Madsen, Henrik; Funder, Simon; Luchner, Jakob; Rosbjerg, Dan; Arnbjerg-Nielsen, Karsten

Publication date:
2014

Document Version
Publisher's PDF, also known as Version of record

Past, present, and future variations of extreme precipitation in Denmark

Technical report

Ida Bülow Gregersen, Maria Sunyer, Henrik Madsen, Simon Funder, Jakob Luchner, Dan Rosbjerg and Karsten Arnbjerg-Nielsen

September 2014

DTU Environment
Department of Environmental Engineering

Past, present, and future variations of extreme precipitation in Denmark
Technical report

Report 1
2014

By
Ida Bülow Gregersen

Cover photo: [Text]
Published by: Department of Environmental Engineering, Miljoevej, Building 113, DK-2800 Kgs. Lyngby, Denmark
Request report from: www.env.dtu.dk

ISBN: [978-87-92654-94-6] (electronic version)

Preface

The present report is prepared as a part of the project “Precipitation in a future climate” supported by the Foundation for Development of Technology in the Danish Water Sector (In Danish: Vandsektorens Teknologiudviklingsfond), contract no. 7492-2012. The data analyses presented here is carried out by DTU Environment and DHI. The main results have served as input to two case studies on risk change accomplished by Greve-Solrød utility company, Aarhus Water, DHI and Krüger, which all have been involved in the overall project. The project has partly been running alongside two PhD projects at DTU Environment, “Statistical modelling of climatic extremes in the hydrological cycle” by Ida Bülow Gregersen, and “Uncertainty analysis of extreme precipitation under climate change conditions” by Maria Sunyer. The first is part of the “Centre for Regional Change in the Earth System” (http://cres-centre.net/) project, the second is part of RiskChange (http://riskchange.dhigroup.com) project, both supported by the Danish Strategic Research Council. The PhD projects have contributed to the results and conclusions presented in the present report.

The project results are also published in two conference papers presented on the 13th International Conference on Urban Drainage, Sarawak, Malaysia (Gregersen *et al.* submitted a and Sunyer *et al.* submitted) and four journal papers (Arnbjerg-Nielsen *et al.* in prep., Gregersen *et al.* submitted b, Madsen *et al.* in prep. and Sunyer *et al.* in review a). All are marked in bold in the reference list.

The analysed data have been provided by the Water Pollution Committee of The Society of Danish Engineers, the Danish Meteorological Institute, Lars Bengtsson at Department of Water Resources Engineering, Lund University, Sweden, the Royal Meteorological Institute of Belgium and the European ENSEMBLES project.

The authors thank the working group behind the project “Precipitation in a future climate” and Søren Liedtke Thorndal, AAU, Department of Civil Engineering for proofreading and constructive comments.

The report serves as a technical report for ‘Skrift 30’ published by the Water Pollution Committee of the Society of Danish Engineers.

Lyngby, July 2014
The Author Team

Summary

The objective of the study was to analyse past, present and future variations of extreme precipitation in Denmark and use the knowledge to review the present guidelines for urban designers.

An updated regional model for estimation of design precipitation was suggested. The model was built on data from the rain gauge network maintained by the Water Pollution Committee of the Society of Danish Engineers. As a new feature, data from the national rain gauge network owned by the Danish Meteorological Institute was also included, greatly improving the description of the regional variations. Comparing the updated model to the old recommendations the change in design intensity varies both with the duration, return period and location in Denmark. For a 2-year event the change ranges from -9% to 26% and results both from the new regionalization and a general increase in the design precipitation intensities. The general increase observed during the last 34 years of observation was further investigated and compared to variations of extreme precipitation in long historical records from the Danish Meteorological Institute going back to 1874. By use of a 10-year moving average a multidecadal pattern of variation was found in the number of extreme events. The pattern showed an increasing phase in the eastern part of Denmark in the last decades. Hence, it is very likely that the general increase in the design precipitation intensities observed over the last 34 years is dominated by natural variability. The analysis furthermore showed that 34 years of measurement is sufficient to reflect the range of natural variability. The updated regional model can therefore serve as a present baseline for extreme design precipitation, to which the guidelines for future changes can be added.

Future changes in design precipitation were evaluated from 13 climate model simulations from the European ENSEMBLES database and several high-end scenarios. Three different methods were applied to downscale the output from the climate models: A delta change approach for extreme events, a stochastic weather generator followed by temporal disaggregation and the climate analogue method. From these a range of climate factors was estimated, which reflect the climate model uncertainty, the variation over Denmark, the uncertainty of the future climate forcing scenario and the uncertainty of the applied downscaling method. This allowed for a selection of standard climate factors that represents the best estimate of the expected future changes. These are 1.2, 1.3 and 1.4 for a 2- , 10- and 100-year event, respectively, for a projection period of 100 years. Additionally, high climate factors that represent the upper 84%-quantile of the expected future changes were estimated. These are 1.45, 1.7 and 2.0 are recommended for a 2- , 10- and 100-year event, respectively.

A stochastic weather generator followed by temporal disaggregation was used to simulated high-resolution precipitation series for two set of future conditions, which represent changes in extreme precipitation characteristics given by the standard and the high climate factors. However, it was found that some of the sub-daily precipitation properties in the synthetic were unrealistic in comparison to observed precipitation. The synthetic series can therefore not be used for urban drainage design.

The updated regional model and the climate factors are published as guidelines for urban designers in ‘Skrift 30’ by the Water Pollution Committee of the Society of Danish Engineers

Content

1. Introduction

1.1 Background

The Water Pollution Committee of the Society of Danish Engineers (WPC) has since the 1950s published a series of guidelines regarding urban design practice. Guideline no. 26 from 1999 (WPC 1999) presents a regional extreme precipitation model for Denmark based on analysis of data from the regional rain gauge network (SVK) also maintained by WPC. The model was updated in Guideline no. 28 in 2006 (WPC 2006) leading to a general increase of the recommended design intensities. The first guidelines on how the uncertainty of the future climate can be incorporated in urban design practice came in Guideline no. 27 in 2005 (WPC 2005) and were followed by specific recommendations on the magnitudes of change in Guideline no.29 in 2008 (WPC 2008). Here changes of +20%, +30% and +40% for a 2- , 10- and 100-year event, respectively, were recommended. The knowledge and focus on the link between anthropogenic climate change and design precipitation extremes have advanced rapidly over the last five years. All motivated by an improved understanding of the earth system, increased computational capabilities allowing for a rapid increase in the number of simulations by global and regional climate models, and increasing public awareness of potential future changes driven by numerous observations worldwide indicating changes in the climate system (e.g. Westra *et al.* 2013). The latter is especially relevant for Denmark where several major pluvial floods have occurred within the last decade. It is therefore highly relevant to update the recommendation to include the latest advancements in understanding of climate change and climate variability.

1.2 Project objective

The present study presents the results of a coordinated effort to review the present guidelines for urban designers in Denmark in the light of the additional years of measurements as well as the newly available climate model simulations and the latest advancements within the field. The main three focus points are:

1) Evaluating and understanding the current increase in the design precipitation intensities and thereby establishing the present baseline for extreme design precipitation, to which the guidelines for future changes can be added. To accomplish this objective it is necessary to revisit historical observations of precipitation.
2) Estimating the projected changes in design precipitation based on state-of-the-art climate model simulations, including an assessment of the uncertainty by providing both most likely and high-end scenarios.
3) Providing simulated high-resolution precipitation series for future conditions, which represent the likely changes in extreme precipitation characteristics.

1.3 Report overview

The project is made at DTU Environment in collaboration with DHI and builds on the knowledge on climate change and variation of extreme precipitation generated at the two research institutions during the last five years. The present report therefore covers a large number of methodologies and datasets. The contribution can be divided into several independent studies, of which some are submitted as scientific papers to international journals directly as an outcome of the project. Results from other existing publications are also included if they provide significant information with respect to the project objectives. Table 1 shows the main tasks and outputs of the project, and in which sections of the report the datasets, methods and results are described.

Table 1: The different datasets, the methods in which they have been applied and the main outputs. DC denotes the delta change approach for extremes, WG denotes synthetic weather generator, disagg denotes the random cascade disaggregation model, and CA the climate analogue method. The sections in which the datasets are descripted are listed to the left, the sections in which the methods are described are listed at the top, while sections in which the results are described are listed at the bottom. The datasets written in grey are high-end climate scenarios, included in the choice of climate factors but analysed and documented elsewhere.

				Climate factors				
		Trends	**Regional extreme precipitation**	DC	WG	WG+disagg	CA	**Future time series**
		Section 3.3	Section 3.2	Section 3.5	Section 3.6.1	Section 3.6.2	Section 3.7	Section 3.6.2
SVK gauge 1979-2012	Section 2.1	Regional trend	Regional model			Calibration		Calibration + validation
DMI gauge 1874-2010	Section 2.2	Natural variation						
DMI gauge 1961-2010	Section 2.3	Natural variation						
DMI grid 1989-2010	Section 2.4		Explanatory variable		Calibration	Calibration		Calibration
E-OBS grid 1951-2012	Section 2.5						Selection of predictor regions	
ENSEMBLES 1950-2010								
daily	Section 2.6			*CF* daily 25x25km^2	*CF* daily 10x10km^2	*CF* hourly 10x10km^2	*CF* daily + hourly point	30 min 10x10km^2
1 hour max	Section 2.6			*CF* hourly 25x25km^2				
1 hour	Section 2.6			*CF* hourly 25x25km^2				
RCP 1981-2100	Section 2.7							
6° scenario 1976-2100	Section 2.7							
		Section 4.2	Section 4.1	Section 4.5 Section 4.6	Section 4.3 Section 4.5 Section 4.6	Section 4.3 Section 4.5 Section 4.6	Section 4.4 Section 4.5	Section 4.7

2. Datasets

Datasets 1 – 3 are point measurements, while 4 – 7 are gridded data sets, i.e. spatially aggregated values.

2.1 SVK high-resolution rain gauges 1979-2012

The SVK rain gauge network has provided the data for the two earlier publications from WPC on regional variation of extreme precipitation. These high-resolution tipping bucket rain gauge stations have a data resolution of one minute and 0.2 mm. The network is operated by WPC and the Danish Meteorological Institute (DMI), see Figure 1 for distribution of the stations over Denmark and Appendix 1 for detailed station information. The data have been quality checked, partly by the DMI and partly by the authors. Presently, 83 of the stations have a total observation period of more than 10 years, and these stations are included in the analysis. For the distribution of stations according to the years of observation, see Figure 2. When periods of rain gauge malfunction have been taken into account, the total dataset corresponds to 1881 station-years. The following variables are defined from the SVK precipitation series: Precipitation intensities with a duration of 1, 2, 5, 10, 30, 60, 180, 360, 720, 1440, 2880 min, accumulated daily precipitation and basin volume 1 and 2 (for definition see Madsen 1998).

Figure 1: The location of the 83 SVK high resolution rain gauges with measurements from 1979-2012

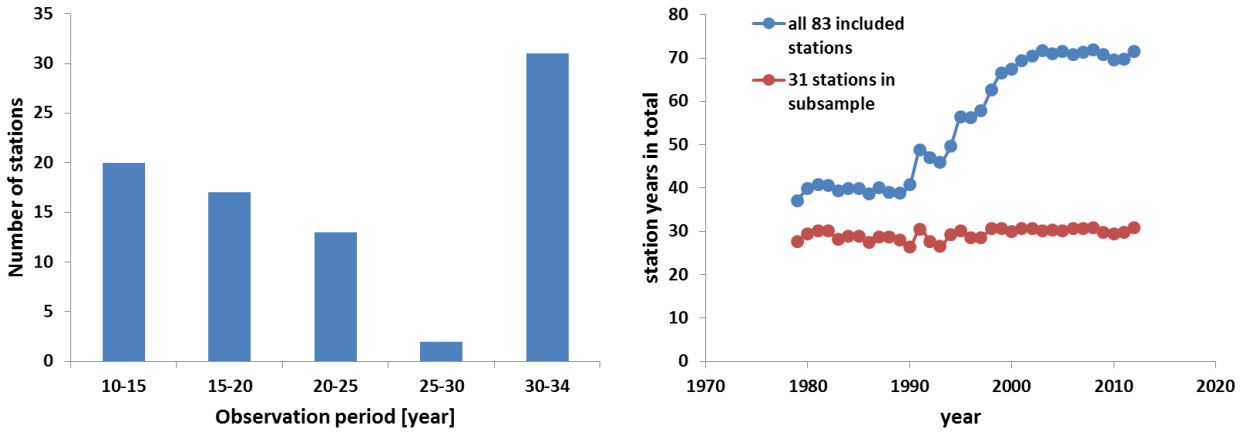

Figure 2: Number of stations grouped with respect to the length of the observation period for SVK stations (left) and the development of the total number of station years during the observation period (right). The subsample of 31 stations is described in Section 4.2

2.2 DMI daily rain gauges 1874-2010

Five series with daily measurements in the period 1874-2010 are available from DMI, see Figure 3. The measurements originate from manual Hellmann gauges with a precision of 0.1 mm. The registration of accumulated diurnal precipitation is made each morning. Only two of the five gauges, Fanoe and Vestervig, have maintained the exact same location during the 137 years of measurement. The rain gauge at Samsoe was relocated in 2001, whereas the series for Bornholm and Copenhagen (Kbh) are assembled by measurements from two and three geographically close stations, respectively. In the assembling procedure one of the available daily measurements is chosen randomly, whenever overlapping measurement periods exist. It has been verified that different realizations of the assembled series give similar results in the performed analyses.

The five final series have days with missing measurements that constitute at a maximum 2.5% of the total series. In the analysis, days with missing measurements are treated as dry days. As a supplement to the long Danish records, one series with daily measurements from Lund, Sweden, covering the period 1874-2010, is also analysed. For further details see Gregersen *et al.* (submitted b).

2.3 DMI daily rain gauges 1961-2010

96 series with daily measurements in the period 1961-2010 are available from DMI. The measurements originate from manual Hellmann gauges identical to those described in Section 2.2. The length of the series differs, but all have at least 45 years of continuous observation. 56 of the 96 stations have been approved by a homogeneity test performed by DMI, where the observed accumulated precipitation is compared to interpolated accumulated precipitation obtained from the surrounding stations (Lundholm and Cappelen, 2010). Data from the 56 stations are included in the analysis (see Figure 3).

Figure 3: The location of the five DMI stations with daily measurements from 1874-2010 (white dots), the single Swedish station with daily measurements from 1874-2010 (white triangle) and the location of the 56 DMI stations with daily measurements from 1961-2010 (black dots).

2.4 DMI climate grid 1989-2010

The Climate Grid Denmark (CGD) dataset from DMI is a gridded data set of daily precipitation which has a spatial resolution of 10x10 km^2 and covers the time period 1989-2010 (Scharling, 2012), see Figure 4a for coverage over Denmark. The grid values are estimated from point measurements obtained from the regional network of daily precipitation stations owned by DMI using an inverse distance weighting method. The daily precipitation provided by Scharling (2012) is not corrected for the wind-induced under-catch or the wetting and evaporation loss. A description of applicable correction procedures for the CGD precipitation values is given in Scharling and Kern-Hansen (2000). In the current project non-corrected values are applied. This does introduce an error, but for most applications related to urban drainage design it is assumed to be minor.

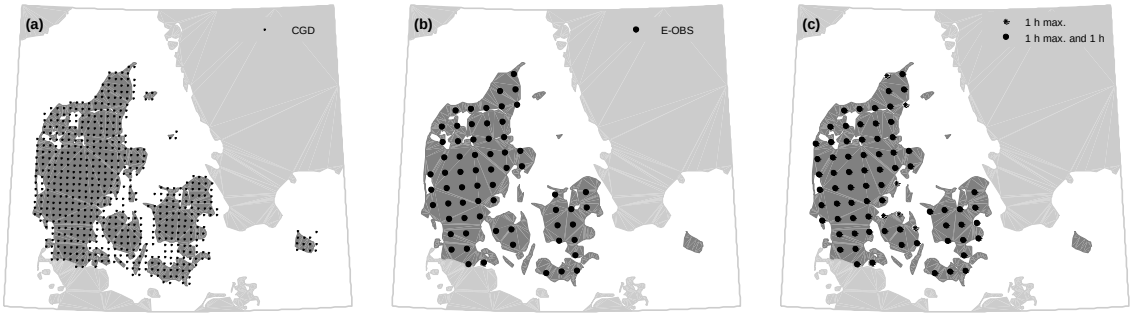

Figure 4: Applied model grids over Denmark. (a) CGD (b) E-Obs (c) ENSEMBLES, daily and 1 hour max are extracted at the same grid points, while the grids for 1 hour and 1 hour max differs as the 1 hour grid was defined prior to the project.

2.5 E-OBS climate grid 1951-2012

The E-OBS dataset was created as part of the ENSEMBLES project (see section 2.6) to provide a dataset for evaluation of climate model performance. It is a gridded dataset of daily precipitation, which has a spatial resolution of approx. 25x25 km and covers the time period 1951-2012. The grid values are estimated from point measurements obtained from the large European ECA&D database using a kriging interpolation method, see Sunyer *et al.* (2013) for more details and Figure 4b for coverage over Denmark

2.6 ENSEMBLES climate model simulations 1950-2100

The climate models used in this study are Regional Climate Models (RCMs) driven by different Global Climate Models (GCMs) from the ENSEMBLES project (van der Linden *et al.* 2009). The goal of the ENSEMBLES project was to estimate the uncertainty in climate model projections. From the project a relatively large ensemble of RCMs was made available; they have a spatial resolution of 25 km and available data up to the end of the century (simulation period 1950-2100).

Table 2: Applied climate models simulations from the ENSEMBLES database

RCM	GCM	Data resolution	Institute
HIRHAM5	ARPEGE	1 hour max, daily	Danish Meteorological Institute
HIRHAM5	ECHAM5	1 hour, 1 hour max, daily	
HIRHAM5	BCM	1 hour max, daily	
REMO	ECHAM5	1 hour max, daily	Max Planck Institute for Meteorology
RACMO2	ECHAM5	1 hour, 1 hour max, daily	Royal Netherlands Meteorological Institute
RCA	ECHAM5	1 hour max, daily	Swedish Meteorological and Hydrological Institute
RCA	BCM	1 hour max, daily	
RCA	HadCM3Q3	1 hour max, daily	
CLM	HadCM3Q0	1 hour max, daily	Swiss Federal Institute of Technology, Zürich
HadRM3Q0	HadCM3Q0	1 hour max, daily	UK Met Office
HadRM3Q3	HadCM3Q3	1 hour max, daily	
HadRM3Q16	HadCM3Q16	1 hour max, daily	
RCA3	HadCM3Q13	1 hour max, daily	Community Climate Change Consortium for Ireland

The information used from these RCMs is daily precipitation and 1h maximum daily precipitation. The latter is only available from 13 out of the 15 ENSEMBLES simulations. For simplicity, the present project estimates the prediction uncertainty from these 13 models only. In addition, two of the ENSEMBLES RCMs have been made available at 1 hour resolution. The RCM/GCM combinations and their data resolution are given in Table 2. All GCMs are forced by the A1B scenario (IPCC 2000). The coverage of the model grid over Denmark is given in Figure 4c.

2.7 High-end scenarios 1976--2100

The A1B scenario forcing the ENSEMBLES is relatively optimistic in terms of projected greenhouse gas (GHG) emissions, when seen in relation to our current emission rate (Peters *et al.* 2013). Hence, the results from several high-end scenarios need to be included in the assessment of future change of extreme precipitation. For Denmark two high-end emission scenarios are currently available, RCP8.5 and 6°, see Table 3. To estimate the relative effect of the high-end scenario, it is compared to a mean climate change scenario, which has been processed in a similar manner. For this purpose RCP4.5 has been selected. In comparison to the old but well-known SRES scenarios (IPCC 2000), the CO_2 emission rate by 2100 in RCP4.5 and RCP8.5 corresponds to B1 and A2, respectively (van Vuuren *et al.* 2011). The general motivation for the new RCP (Representative Concentration Pathways) scenarios, where the forcing effects of the emitted greenhouse gasses is central instead of the socio-economic development of the world, is discussed in detail in Moss *et al.* (2010). In the 6° high-end scenario, the average global temperature increase is in focus, and the scenario is constructed to reach 6°C in 2100 (Christensen *et al.* submitted).

The model setup using the RCP8.5 and RCP4.5 as climatic forcing outlined in Table 3 is described in detail by Mayer *et al.* (submitted). The RCM outputs have been further downscaled by Sørup *et al.* (in prep.) using a weather generator, which partly resembles the one described Section 3.6.1, but with a spatial module and calibrated to point precipitation. The model setup using the 6° and RCP4.5 as climatic forcing outlined in Table 3 is described in detail by Christensen *et al.* (submitted). The RCM outputs have been further downscaled by Arnbjerg-Nielsen *et al.* (submitted) using a delta change approach identical to the one described in Section 3.5.

Table 3: Information on high-end scenarios

Name	RCM	GCM	Temporal resolution	Spatial resolution	Present period	Future period	Downscaling
RCP8.5	HIRHAM 5 (Christensen *et al*. 2007),	EC-EARTH (Hazeleger *et al*. 2012)	1hour	8 km	1981-2010	2071-2100	advanced weather generator
RCP4.5	HIRHAM 5 (Christensen *et al*. 2007),	EC-EARTH (Hazeleger *et al*. 2012)	1hour	8 km	1981-2010	2071-2100	advanced weather generator
6°	HIRHAM 5 (Christensen *et al*. 2007),	EC-EARTH (Hazeleger *et al*. 2012)	1hour max/ daily	25 km	1976-2005	2071-2100	Delta change
RCP4.5	HIRHAM 5 (Christensen *et al*. 2007),	EC-EARTH (Hazeleger *et al*. 2012)	1hour max/ daily	25 km	1976-2005	2071-2100	Delta change

3. Methods and definitions

3.1 Partial Duration Series and Extreme Value Theory

The extreme value analysis follows the theory of Partial Duration Series (PDS) where the annual number of extreme events (*N*) is assumed to follow a Poisson distribution and the magnitude of the extreme events is assumed to follow a Generalized Pareto distribution (GPD) (Rosbjerg *et al.* 1992; Willems *et al.* 2012). Therefore a T-year event (z_T) is estimated by:

$$z_T = z_0 + \mu \cdot \frac{1+\kappa}{\kappa}\left[1 - \left(\frac{1}{\lambda T}\right)^{\kappa}\right] \qquad \text{where} \qquad \kappa = \frac{1}{L_{cv}} - 2$$

The parameters in the equation are denoted; the location parameter (z_0), the shape (κ) parameter, the mean of the extreme exceedances (μ), the L-moment coefficient of variation (L_{cv}) and the average annual number of extremes (λ) which corresponds to the rate parameter of the Poisson distribution

When sampling the extreme events from a time series, the PDS approach offers two censoring methods. In type 1 censoring, the threshold over which an event is considered as extreme is pre-fixed. The method is also known as Peak over Threshold (POT) (Coles 2001). Note that the threshold is equivalent to z_0 of the GPD. In type 2 censoring, λ, and thereby the total number of extremes during the observation period, is pre-fixed. The optimal choice of censoring methods depends on the data and the nature of the analysis. In the regional PDS model developed by Madsen and Rosbjerg (1997) type 1 censoring was used. This model is considered as state-of-the-art and is applied in the current description of extreme precipitation in Denmark (Madsen *et al.* 2002; Madsen *et al.* 2009). However, when regionalization is not the goal of the analysis, or when the variation within the data set is too large for a common threshold to be found, type 2 censoring can be more suitable. Larsen et al. (2009) applied type 2 censoring when analysing changes in extreme precipitation over Europe, as projected by a RCM.

The extreme events in the PDS are required to be independent (Coles 2001). In the literature there are at least two common ways of ensuring this. Madsen *et al.* (2002) performed an event-based separation, where each extreme belongs to a specific precipitation event defined by a start and end time. For the events to be independent the dry weather period between two precipitation events must be longer than or equal to the duration. A more simple approach, often applied in analysis of daily RCM projections, is to consider the occurrence of the extremes and sample events separated by a given time window. In this study, the difference between the two methods is considered negligible.

Table 4 shows the combination of dataset and methods (with reference to Table 1) in which extreme value analysis has been applied, together with the applied censoring method and independence criteria.

Depending on the censoring method, either λ or z_0 is regarded as a stochastic variable which can be estimated from the dataset together with *α* and *κ*. The method of L-moment is applied for the estimation (Hosking and Wallis 1993; Willems *et al.* 2012). The estimation uncertainty on *κ* is large. This uncertainty can be reduced by assuming that L_{cv} is homogenous over a larger region (Madsen *et al.* 2002).

Table 4: PDS censoring and independence criteria used for the different datasets * See Sørup et. al. (in prep) for details

Dataset	Method	PDS censoring	Independence
SVK 1979-2012	Trends and regional model	Type 1	Independent precipitation events
DMI 1874-2009	Trends	Type 1	Independent precipitation events
DMI 1961-2009	Trends	Type 1	Independent precipitation events
ENSEMBLES daily precipitation	DC	Type 2	24 hours distance
ENSEMBLES daily precipitation	WG	Type 2	24 hours distance
ENSEMBLES daily precipitation	WG + Disagg	Type 2	24 hours distance
ENSEMBLES daily 1 hour max	DC	Type 2	24 hours distance
ENSEMBLES hourly precipitation	DC	Type 2	Independent precipitation events
High-end scenario 6^{o} and RCP4.5	DC	Type 2	Independent precipitation events
High-end scenario RCP8.5 and RCP4.5	WG*	Type 1*	Independent precipitation events*

3.2 Regional extreme value modelling

The regional extreme value model developed for estimation of Danish precipitation extremes by Madsen *et al.* (2002) is applied in this study. The model combines PDS of precipitation extremes from all 83 SVK rain gauges for estimation of regional IDF relationships and other precipitation characteristics. In this section a brief description of the regional model is given. The reader is referred to Madsen *et al.* (2002) for a more detailed description.

In the regional PDS model the λ, μ and L_{cv} are taken as regional variables. The regional modelling includes the following steps (Madsen *et al.* 2002):

(i) Evaluation of regional homogeneity of the three parameters.
(ii) For parameters showing regional heterogeneity, evaluation of the potential of describing the regional variability from physiographic and climatic characteristics.
(iii) Determination of a regional extreme value distribution.

In the previous regional studies of Danish precipitation extremes (Madsen *et al*. 2002; Madsen *et al*. 2009) it was found that the λ has a significant regional variability and a large part of this variability can be explained by the mean annual precipitation (MAP), i.e. the larger MAP the larger frequency of extremes. The correlation with MAP is more pronounced for larger rainfall durations.

For μ the regional variability increases for increasing duration, and for durations larger than 3 hours a spatial pattern could be identified with larger extremes in the Eastern part of Denmark. In the first study by Madsen *et al*. (2002) the increase in mean intensity was mainly seen in the Copenhagen area, and a regional model was defined with three sub-regions, respectively, (i) Copenhagen East, (ii) Copenhagen West, and (iii) the rest of the country. In the subsequent study by Madsen *et al*. (2009) the regional model was revised, and two sub-regions were defined, west and east of the Great Belt.

For L_{cv} (defining κ of the GPD) the analysis showed for most durations that the region can be considered homogeneous, and hence a regional estimate of L_{cv} can be applied (corresponding to a κ). Analysis of different regional statistical distributions showed that the generalised Pareto distribution provides the best fit.

3.3 Trends and multidecadal oscillations

The non-stationary characteristics of the extreme precipitation can be evaluated on an annual basis, either for each station/grid cell independently or for regional averages over Denmark. Following the procedure described by Gregersen *et al*. (2013), where the extreme values are censored by a type 1 PDS procedure, the temporal annual development in λ and μ is modelled by regional averages. The trend over time (t_y) is described by Poisson regression for λ and ordinary linear regression for μ:

$$\lambda = \exp(a_\lambda + b_\lambda t_y + \varepsilon_\lambda)$$
$$\mu = a_\mu + b_\mu t_y + \varepsilon_\mu$$

Where *a* and *b* are regression parameters and ε the regression error, see Gregersen *et al*. (2013) for details.

Due to the highly variable nature of precipitation extremes it can be difficult to separate long term trends from random variations, when the evaluations are made on an annual basis. Ntegeka and Willems (2008) applied a moving window of 5-15 years as a filter to enhance the multidecadal signal for extreme precipitation variations. The filter can be expressed as a perturbation factor (*pf*) where a selected extreme value characteristic ($C_{extreme}$) is calculated for both the subseries (t_{sub}), defined by the moving window, and the full series (t_{full}):

$$pf = \frac{C_{extreme}(t_{sub})}{C_{extreme}(t_{full})} \quad (1)$$

As $C_{extreme}$ we chose λ and μ. The method requires an observation period of several decades.

3.4 The climate factor

Changes in extreme precipitation characteristics are here quantified using climate factors (*CF*). The *CF* for a given T-year event, location, *l*, and precipitation duration, t_c, is defined as

$$CF_{T,l,t_c,\Delta t} = \frac{z_{T,l,t_c,t+\Delta t}}{z_{T,l,t_c,t}}$$

where *t* is present time, and Δt represents the length of the projection period. Often a *CF* is assumed constant over a larger area, which means that it will only vary as a function of return period, projection period and potentially the duration of the precipitation.

The *CF* is based on the widely used delta change methodology, which can be applied to all climatic variables simulated by the RCMs. The output of the state-of-the-art RCMs has a different spatial scale than the precipitation series of point measurement used for estimation of urban design intensities. Hence the RCM output must be downscaled to obtain a *CF*, which can be applied to estimate future design intensities. This study applies three downscaling methods: A delta change method for extreme events, a weather generator combined with a disaggregation method, and a climate analogue method. All methods rely on the assumption that the bias in the RCMs properties will remain constant from present to future.

In the delta change method for extreme events *CF* is calculated from the extreme precipitation simulated by the RCM. Hence, the method depends on the RCM's ability to simulate extreme precipitation. Furthermore, it assumes that the changes at the local scale (being point measurement) are identical to the change at the large scale (given by the spatial resolution of the RCM). For more details the reader is referred to (Sunyer *et al*. in review a; Arnbjerg-Nielsen 2012). The two other downscaling methods do not rely strongly on the RCM's ability to simulate extreme precipitation, but uses other, potentially more robust climatic variables from the projections.

3.5 Delta change approach for extreme events

When the delta change approach is applied on RCM data for estimation of *CF*, extreme precipitation events are sampled for a period representing the present, often referred to as the 'control period' or 'baseline period' (often 1961-1990), and for a period representing the future, often referred to as the 'scenario period' or 'projection period' (Larsen *et al.* 2009). As mentioned in section 3.1, a type 2 censoring is most suited for sampling the RCM simulated extremes. Previous Danish studies (Gregersen *et al*. 2013; Madsen *et al*. 2002) used an average exceedance frequency of 3 events per year. For consistency a type 2 censoring on 30 years of RCM simulated precipitation should extract the 90 largest, independent events in each grid cell. A GDP distribution is fitted to each cell individually and applied to estimate design intensities with different return periods. As mentioned in section 3.1, the estimation uncertainty of the shape parameter is large, and variation of parameter estimates between neighbouring RCM cells often seem unrealistic (Larsen *et al.* 2009). To address this, a regional estimate of the L-coefficient of variation is used, see Section 3.2.

3.6 Stochastic weather generator and temporal disaggregation

The approach described below is both used as a downscaling method to evaluate the changes in extreme precipitation and to generate synthetic high-resolution precipitation series for present and future conditions, which can be used in urban design models. The weather generator (WG) described in Section 3.6.1 is used to spatially downscale the daily 25x25km^2 RCM outputs to 10x10 km^2, while the disaggregation method described in Section 3.6.2 is used to temporally downscale the WG output to 30 minutes.

3.6.1 RainSim

The WG used in this study is included in the software RainSim (Burton *et al*. 2008). RainSim is based on the Neyman-Scott Rectangular Pulse (NSRP) WG (Cowpertwait *et al*. 1996). This type of WG is built on a clustering approach, where precipitation is associated with clusters of rain cells making up storm events. This process fits well with the observed nature of precipitation. The clustering approach leads to the following four steps in the NSRP model (Kilsby *et al*. 2007):

a. A storm origin arrives according to a Poisson process.
b. Each storm origin generates a random number of rain cells according to a Poisson process. Each rain cell is separated from the storm origin by exponentially distributed time intervals.
c. The duration and intensity of a rain cell are independent random variables described by exponential distributions.
d. The total precipitation intensity is the sum of the intensities of all the active cells at that time step.

The parameters of the four processes described above must be calibrated for each specific case study. This can be done for a large number of precipitation statistics. In this project we apply mean, variance, skewness and probability of a dry day. The WG is used to generate 100-year long time series representing current and future climate. The time series for the present are generated using the observed properties from the CGD dataset. To simulate future precipitation, the four selected precipitation statistics are perturbed using the estimated changes from the RCM simulation (see Sunyer *et al.* 2012 for more details).

3.6.2 Temporal disaggregation

Based on a time series of precipitation with a given temporal resolution, it is possible to obtain series of higher resolution by means of temporal disaggregation. The basic assumption is that the properties of precipitation are scalable at resolutions between two days and 30 minutes (Olsson 1998), i.e. their relation can be described by a simple statistical model. Note that the mentioned range depends on the specific climate of the region and should be verified from local precipitation data. One possible way of performing the temporal disaggregation is by the well-documented random cascade model (Molnar and Burlando, 2005). Here each temporal block is split evenly *n* times by a series of cascades until the desired temporal resolution is

achieved. The model is composed of an intermittency factor, which controls the rainy and non-rainy fraction, and a factor which controls the rainfall intensity. The parameters of the cascade generator are estimated from the properties of the sample moments at different temporal scales, which are derived from observed precipitation, and its performance should be validated before it is applied on the series generated by the WG, see Sunyer *et al.* (in review a) for more details.

Four of the rain gauge stations described in Section 2.1 are used for parameter estimation. They represent the variation of extreme precipitation over Denmark, both in terms of their geographical locations and in terms of their extreme precipitation characteristics. The scaling parameters are estimated separately for each season (winter, DJF; spring, MAM; summer, JJA; and autumn, SON) but averaged over the four stations. As validation the four observed precipitation series are aggregated to a daily resolution, disaggregated by the cascade model and compared to the observations.

The WG series for present and future are disaggregated to a resolution of 30 min. Extreme precipitation characteristics are estimated from the generated time series, and *CF*s are then derived using the delta change approach described in Section 3.5. In addition, representative current and future precipitation time series are extracted from the generated time series that reflect current extreme precipitation characteristics and the changes in these for a range of temporal resolutions.

3.7 The climate analogue method

The method of climate analogues uses a set of climate variables to identify locations or regions where the present conditions can resemble the conditions of an otherwise unknown (past or future) state of another location. Obviously, the variables that identify the analogue location must be known to serve as predictors of the anticipated change. In the literature the method is also known as space-for-time (e.g. Refsgaard et al. 2014).

The present study repeats the procedures of Arnbjerg-Nielsen (2012) using an updated and vastly improved dataset of climate model simulations. Furthermore, a metric, which can serve as the anticipated climate change, is developed based on the differences between projected future climate indices in Denmark and the current climate indices throughout Europe. This metric is used to identify suitable locations from which extreme precipitation statistics should be collected. The calculations are performed using newly developed software (Arnbjerg-Nielsen *et al.* in prep.) that uses the E-OBS dataset as a reference for the current European climate indices and the ENSEMBLES climate model simulations) for the future, see Section 2.5.

As predictors for the future climate the program uses:

- Monthly distribution of mean temperature
- Monthly distribution of variance of daily temperature
- Monthly distribution of mean precipitation
- Monthly distribution of variance of daily precipitation
- Monthly distribution of proportion of dry days
- Extreme value statistics (1- and a 10-year event) of daily precipitation

For details on how to combine the six indices into one overall metric and how sensitive the metric is to the choice of weights, see Arnbjerg-Nielsen *et al.* (in prep.). The metric takes values close to 0 for regions which serve as good climate analogues. In the current study mean temperature, mean precipitation and the extreme value statistics were given the highest weights.

4. Results

4.1 Regional extreme value modelling

The threshold values used to define the analysed PDS series are given in Appendix 2, together with all the parameters in the updated regional model descripted below.

The analysis shows that λ can be related to the MAP, see Section 3.2. As was also found in the previous studies, the relationship is more pronounced for larger precipitation durations, see Figure 5, but statistically significant for all the analysed precipitation variables listed in Section 2.1.

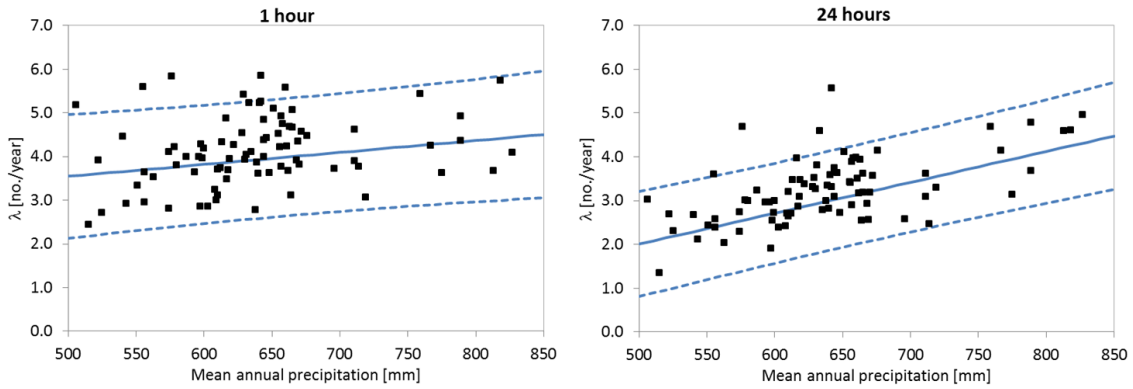

Figure 5: Estimated relations between the mean annual number of extreme events and the mean annual precipitation for durations of, respectively, 1 hour (left) and 24 hours (right). Dotted lines represent the 95% confidence interval of the linear regression.

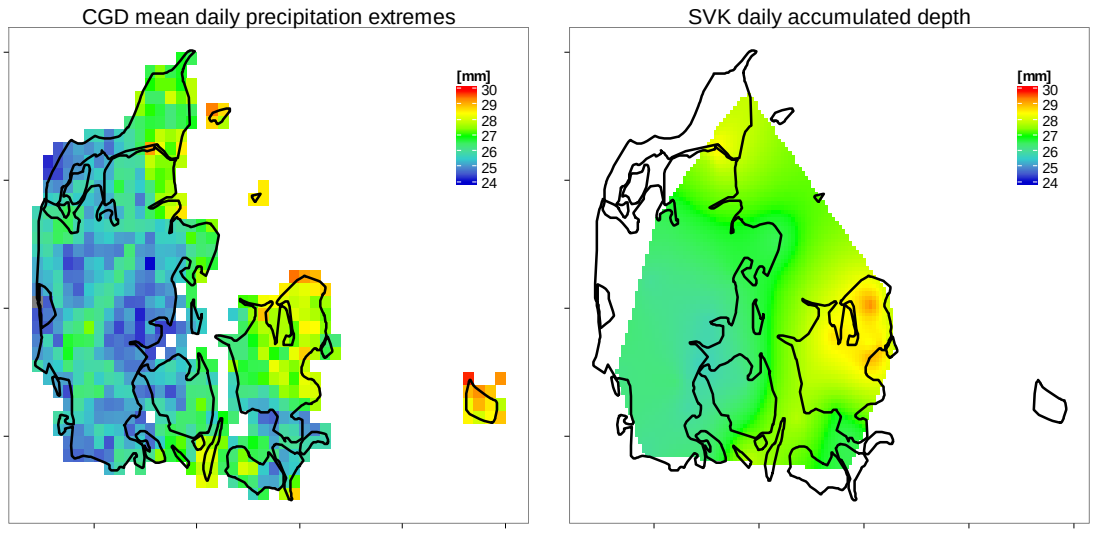

Figure 6: Spatial variation of the mean accumulated daily extreme for the SVK data (left) and mean daily precipitation extreme of the DMI climate grid data (right).

For μ a regional pattern is seen for durations larger than 3 hours, with larger values in the eastern part of Sealand, northern part of Jutland, and southern islands. This regional pattern is also seen in the mean value of the daily precipitation extremes of the CGD data (μ_{CGD}), see Figure 6. In this respect daily precipitation extremes from the CGD have been analysed by the same PDS approach as applied for the SVK data, using 19.2 mm/day as the threshold for extreme daily precipitation.

This motivates a regional regression analysis between μ (for all the analysed precipitation variables listed in Section 2.1) and μ_{CGD}. It was found that for durations larger than 3 hours a significant part of the regional variability of μ can be explained by μ_{CGD}. The correlation is more pronounced for larger durations. For durations smaller than 3 hours, the correlation is not significant and a regional average is applied. Estimated regional regression models for the mean intensity for 1- and 24-hour durations are shown in Figure 7.

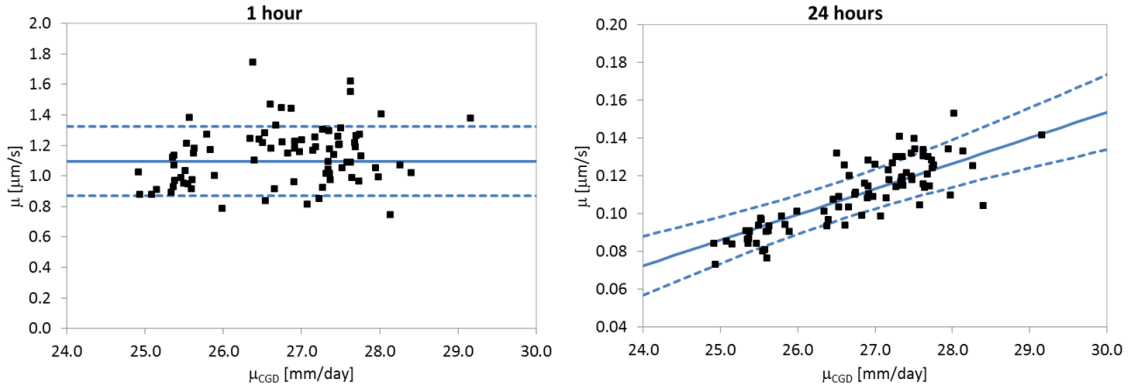

Figure 7: Estimated relations between the mean intensity and the mean daily extreme of the DMI climate grid data for durations of, respectively, 1 hour (left) and 24 hours (right). Dotted lines represent the 95% confidence interval of the linear regression.

For the L-coefficient of variation the regional analysis confirms the results of the previous studies. The L-coefficient of variation can be assumed homogeneous for all the analysed precipitation variables listed in Section 2.1, except for 1 and 2 minutes intensities. Goodness-of-fit analysis of different distributions also confirms the results of previous studies, i.e. the GPD can generally be accepted as regional distribution for all precipitation variables.

Application of the regional model for estimation of extreme intensities is shown in Figure 8. The figure shows estimated extreme intensities for 1- and 24-hour durations mapped on the CGD grid. The explanatory variables used in the regional model are MAP and the μ_{CGD}, which are mapped on the CGD grid in Figure 8 (top row). For durations smaller than 3 hours the regional variability is only due to the variability in λ as explained by MAP (Figure 8 left column), whereas for durations larger than 3 hours the regional variability in the μ as described by μ_{CGD} also contributes to the regional differences in the extreme intensities (Figure 8 right column). For smaller return periods the regional variability in λ has a relatively larger contribution to the regional variability of the extreme intensity, whereas for larger return periods the regional variability in μ dominates.

Figure 9 shows the range of the estimated IDF curves over Denmark for 2, 10 and 100-year return periods. The range is calculated as the minimum and maximum extreme intensity of the different durations from the CGD gridded estimates as shown in Figure 8. The range is smallest for durations up to 1-hour, reflecting the small regional variability of λ (Figure 5 left) and constant μ (Figure 7 left) for these durations. For durations larger than 1 hour the range increases for increasing duration, caused by a more pronounced regional variability of λ (Figure 5 right) and increasing regional variability of μ (Figure 7 right). For durations of 24-48 hours the lower range of the 10 and 100-year events are similar to the upper range of, respectively, the 2 and 10-year events. A regional IDF-curve representing the average design precipitation over Denmark is obtained by taking the average over all grid points, see Figure 9. This curve is applied in Section 4.4 and Section 4.7.

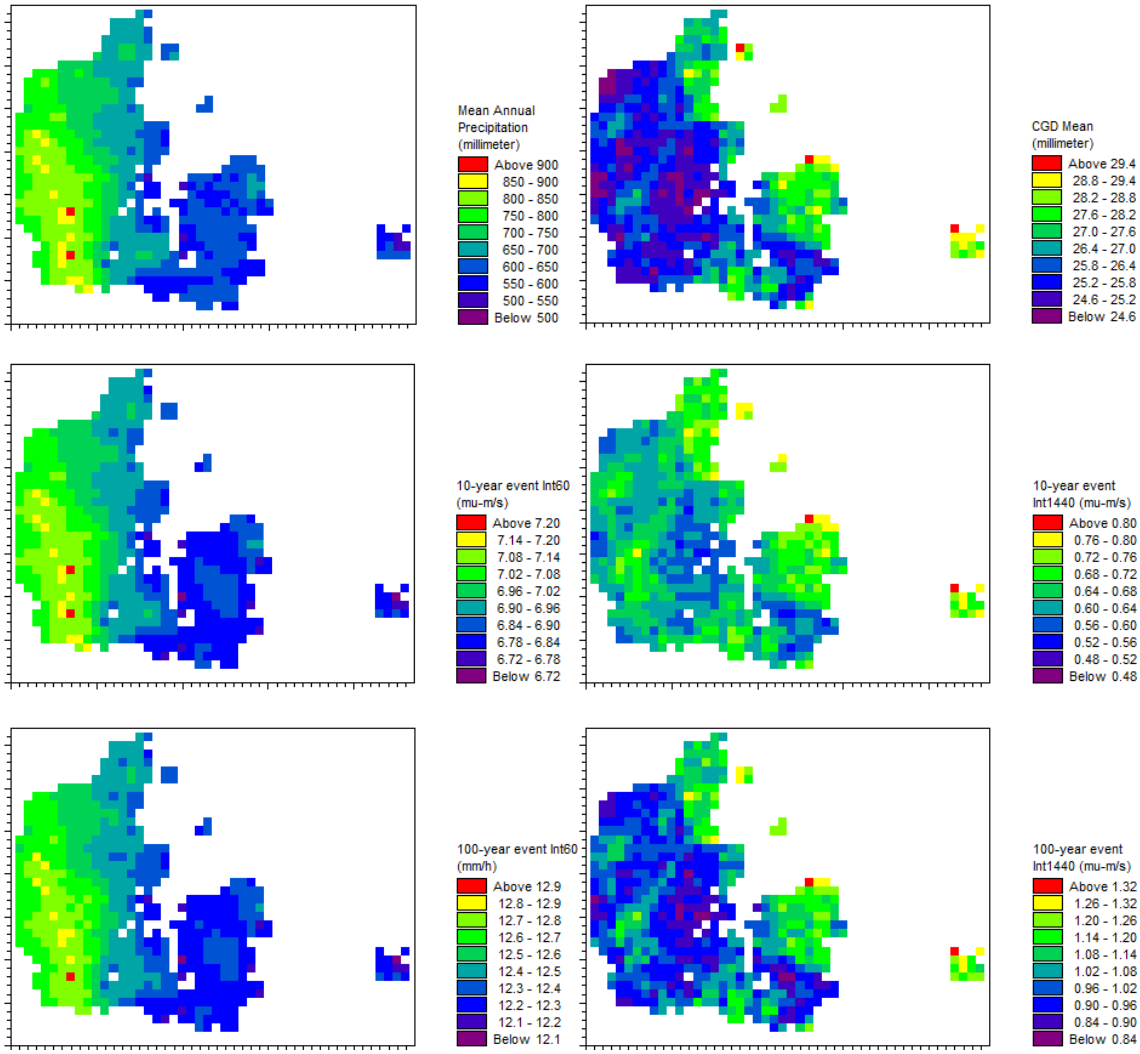

Figure 8: Application of the regional model. Explanatory variables in the regional model (top row), being mean annual precipitation (left), and mean daily extreme of the DMI climate grid (right). Estimated 10-year events (middle row) and estimated 100-year events (bottom row) for 1-hour duration (left column) and 24-hour duration (right column).

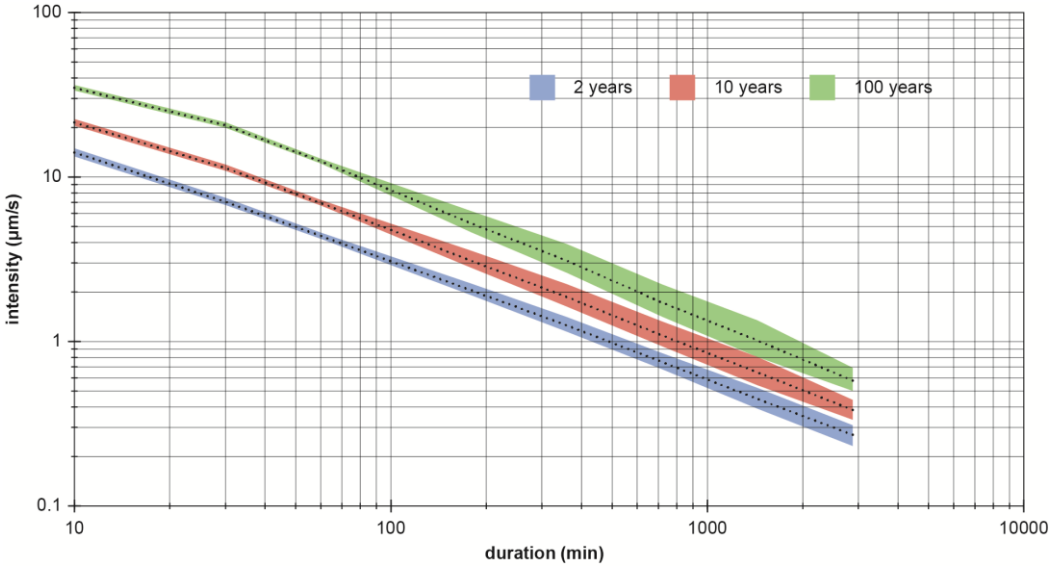

Figure 9: IDF curves for a 2, 10 and 100 year event in blue, red and green, respectively. The area represents the variability over Denmark given by the range of estimated extreme intensities mapped on the CGD grid, while the black lines in the centre of each area represents the average regional IDF-curve.

4.2 Trends and multidecadal oscillations

From the SVK data the non-stationary characteristics of the extreme precipitation is evaluated. By use of the method described in Section 3.3 the temporal development in λ and μ is estimated for the precipitation variables listed in Section 2.1. Plots for all analysed variables can be found in Appendix 3, while the development in λ and μ are shown for durations of 10, 60 and 1440 min in Figure 10 and Figure 11, respectively.

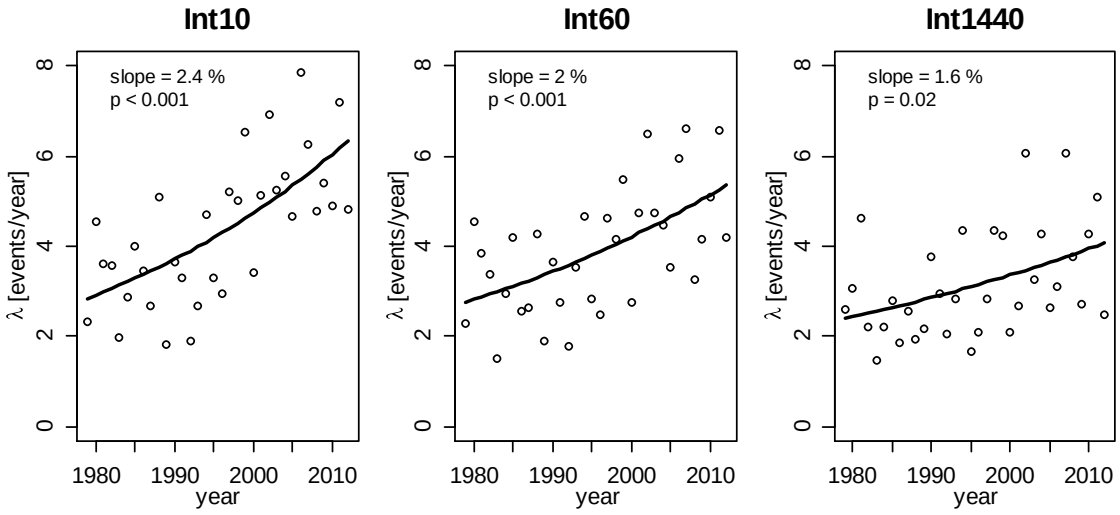

Figure 10: Annual development in the number of extreme precipitation events between 1979 and 2012, calculated as a regional average of all the SVK stations, for rainfall durations of 10 (left), 60 (middle) and 1440 (right) min. Because Poisson regression is applied the slope is given in percentages. *p* denotes the probability of the estimated slope to being equal to zero, if below 0.05 the increase is significant

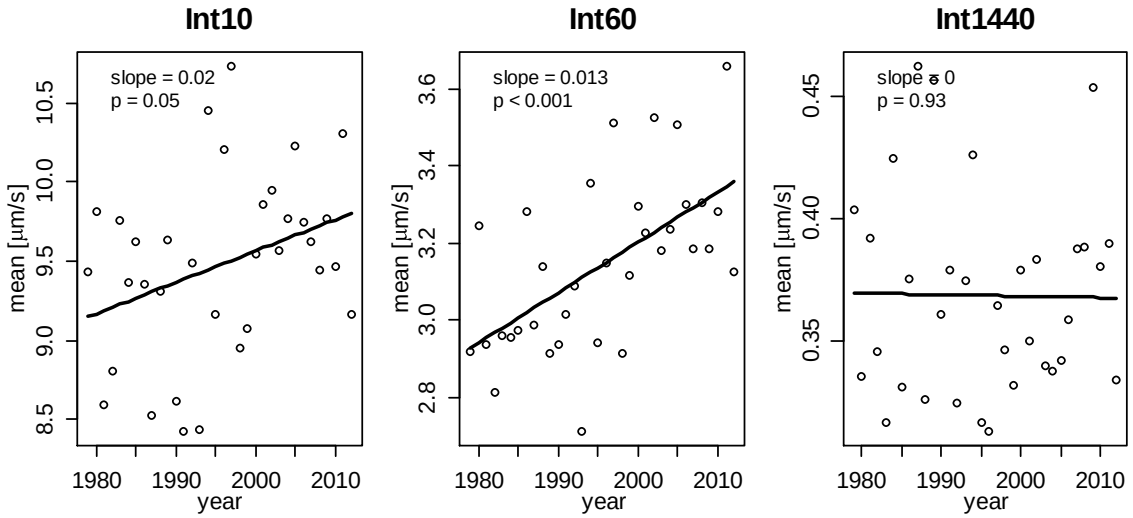

Figure 11: Annual development in the mean intensity of extreme precipitation events between 1979 and 2012, calculated as a regional average of all the SVK stations, for rainfall durations of 10 (left), 60 (middle) and 1440 (right) min. Because linear regression is applied the unit slope is µm/s/year. p denotes the probability of the estimated slope to being equal to zero, if below 0.05 the increase is significant

Using a significance level of 5% a significant increase in λ over the 34 years of observations is found for all precipitation variables given in Section 2.1. The annual increase varies between 1.3 and 2.4 %. Given the uncertainty on the estimated slopes the rate of increase cannot be shown to vary with the duration of the precipitation. μ is found to increase for basin volume 1 and precipitation durations between 10 min and 2 hours. Not surprisingly, the year to year variation is high, but for the variables mentioned above the increase is strong enough to be statistically significant.

The short term increases are compared to the increases in the long DMI series, where only accumulated daily precipitation is available but for 137 years of measurements, see Figure 12 and Figure 13. For λ there is a clear difference in the observed annual increase between the two datasets. The slope of the increase is only 0.3% in the regional average of the five long series. Looking at the regional average of the 56 stations from 1961-2010 the slope increases marginally.

The difference in slope is investigated by applying the modified version of the approach by Ntegeka and Willems (2008) described in Section 3.3 to each of the five series individually. The purpose is both to look for multidecadal temporal variations and regional differences in smoothed series produced by Eq. (1). The result for λ is given in Figure 14. It is seen that the year-to-year variation is high and without clear evidence of persistence. In the smoothed series there seems to be a multidecadal variation that resembles the oscillatory behaviour found by Ntegeka and Willems (2008) and Willems (2013a). Also five out of the six stations show a general increase over time. The periods of high/low λ-values do not show a uniform occurrence all over Denmark, but from Figure 14 it seems that both the series from Fanoe, Vestervig and Kbh have oscillating patterns with a period of 25-40 years, however with differing phases.

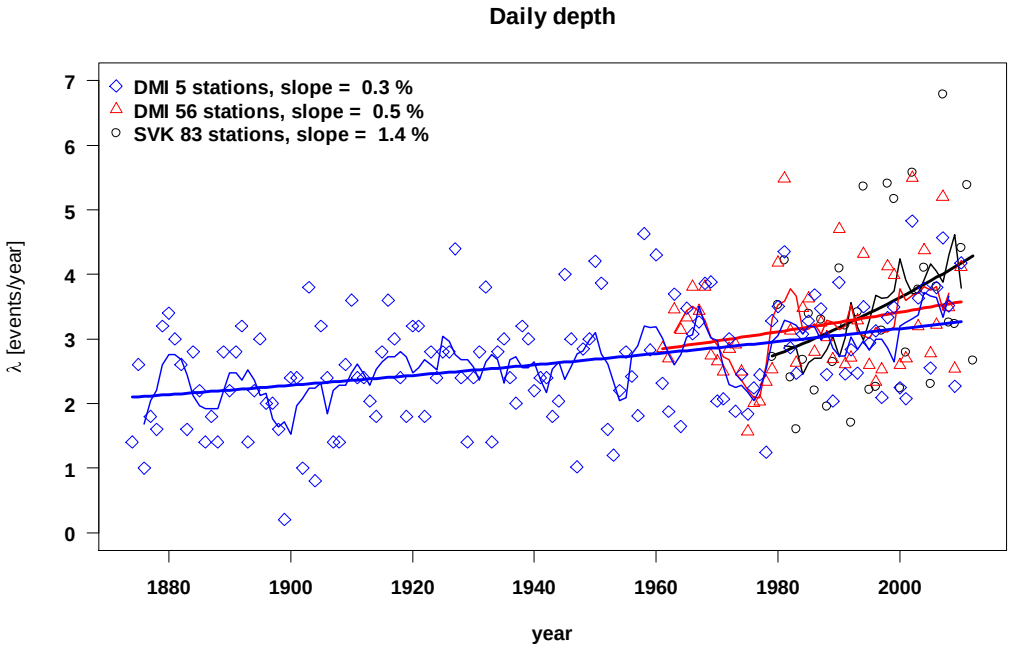

Figure 12: Annual development in λ for accumulated daily precipitation extremes, comparing the regional average of SVK (black), DMI 1961-2010 (red), and DMI 1874-2010 series (blue). Development over time is illustrated by a five year moving average and Poisson regression

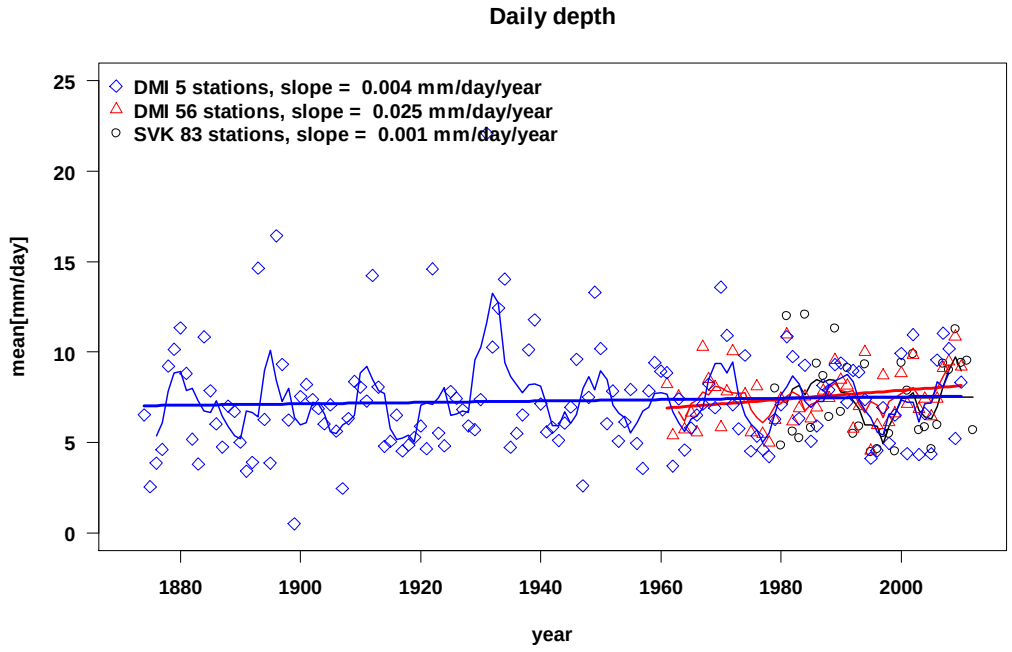

Figure 13: Annual development in the mean intensity of extreme precipitation, comparing the regional average of SVK (black), DMI 1961-2010 (red), and DMI 1874-2010 series (blue). Development over time is illustrated by a five year moving average and linear regression

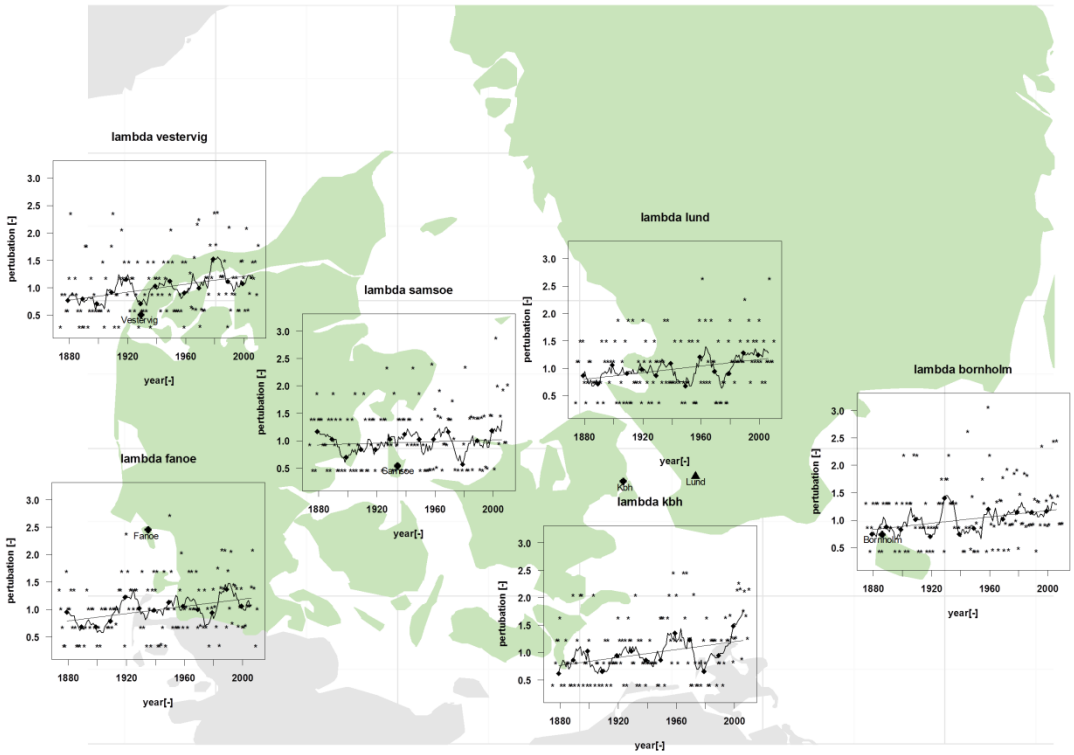

Figure 14: Annual variation in the frequency of extreme events (black dots) and multidecadal variation of the smoothed series based on 137 years of measurements for six stations in Denmark and southern Sweden. The POT threshold is 19.2 mm/day and the window length is 10 years. The figure is adapted from Gregersen et al. (submitted a).

It is generally known that moving windows can introduce artificial oscillations in series of independent and identically distributed random variables and that they introduce autocorrelation in the series. In Figure 15 the autocorrelation in the annual λ series, the *pf* series generated with a window-length of 10 years and the 13 independent points generated by a block average of 10 years are compared for the DMI station in Copenhagen. It is seen that years separated by a lag phase of approximately 20 and 40 have a correlation value that is close to be significant for the annual λ series, see Figure 15 (upper panel). It was also evaluated how the pattern changes with a changing window length (see Appendix 4); using a window length of 3 years the found oscillation signal starts to appear, but it is also clear that the annual λ series contain other periodic components than the one highlighted by the 10 year window. Gregersen *et al*. (submitted a) suggests that spectral analysis based on Fast Fourier Transformation is applied to evaluate the different periodic components of a series; their main result is reproduced in Figure 16. To conclude, the multidecadal variation in the smoothed series with a period of 25-40 years is dominating in the series from Kbh and Bornholm, in the other series it is present but not significant. Any future projections of the variations in λ, including potential significant periodic components, should be based on the full spectrum as discussed by e.g. Lee and Ouarda (2010).

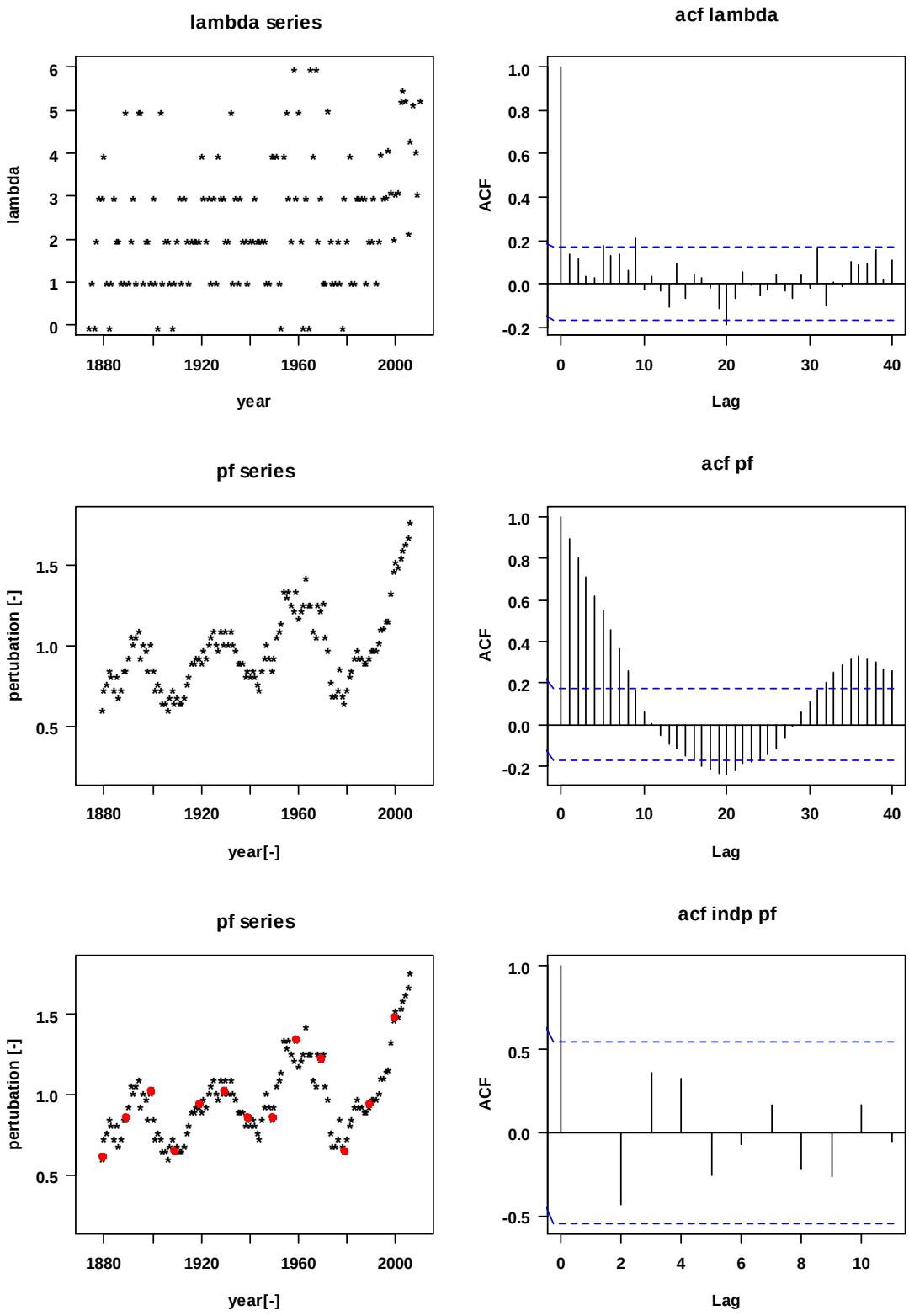

Figure 15: Time series (left) and autocorrelation functions (right) for λ and pf series from Kbh comparing: the raw data (upper panel), the data smoothed by a moving average with a window of 10 years (middle panel) and the 13 independent block averages with a window length of 10 years (lower panel)

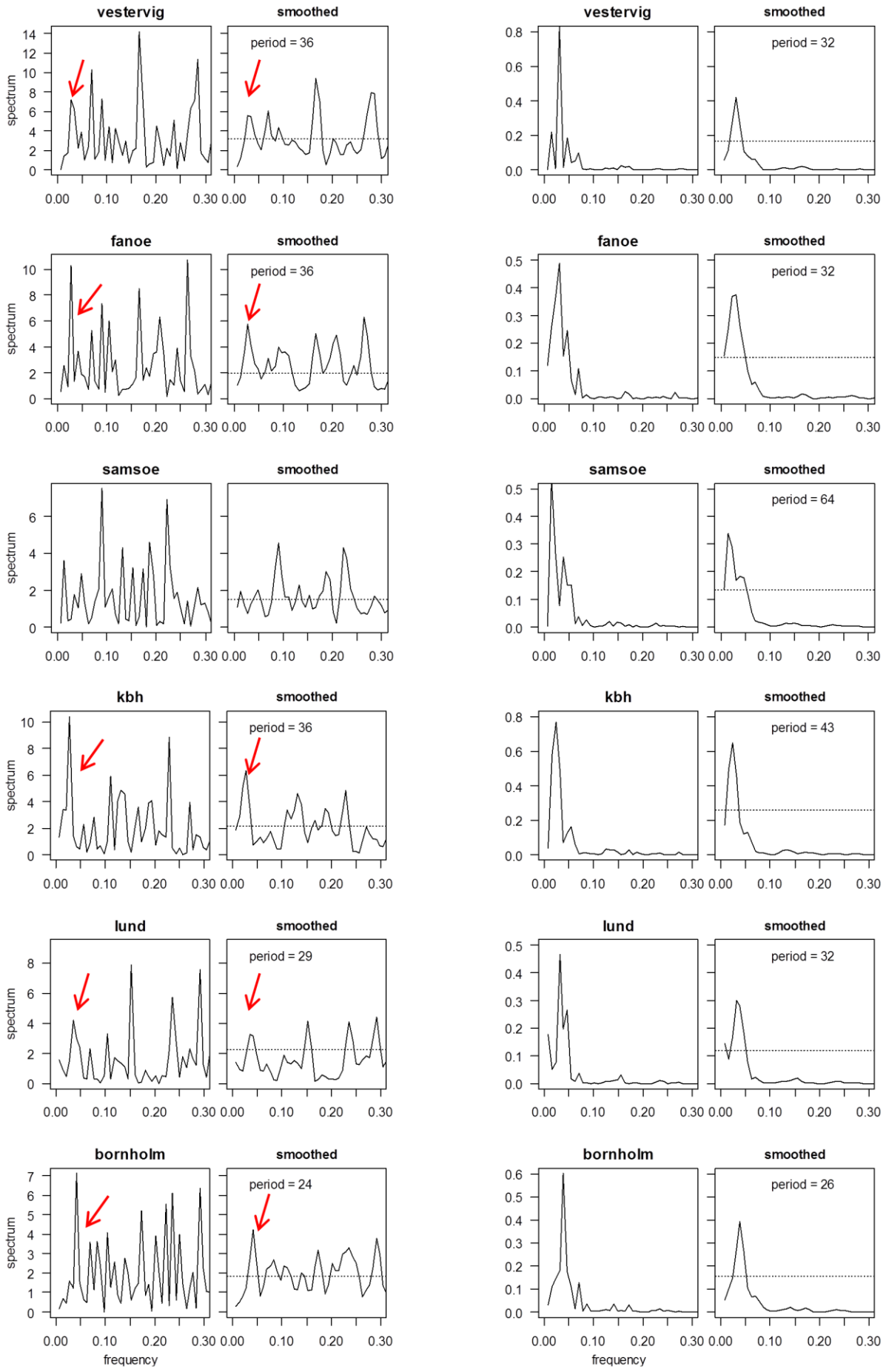

Figure 5: Estimated spectral density for the six linearly detrended series of λ (left column) and the six linearly de-trended series of *pf* (right column). Each plot includes a raw and a smoothed periodogram, for the latter the applied smoothing length is three. The period of the maximum peak of the pf_λ series (right column) is given in years, the corresponding peak in the λ series is marked by red arrows (left column). The horizontal line in the smoothed periodogram represents the lower 95%-confidence interval of the maximum peak. The figure is adapted from Gregersen *et al.* submitted a.

The sensitivity of the results with respect to the POT threshold and the season of occurrences have been analysed. It was found that the oscillations do depend on the season of the extremes. For the station in Copenhagen the majority of the extreme event occurs between May and October. If *pf* is computed for these months only the oscillation signal prevails while the general increase diminish. For the west coast stations the signal is less clear when focusing on different seasons, but the general increase is also prevailing in the winter months. The pattern changes with the threshold, in general it becomes stronger when the threshold increases and weaker when the threshold decreases.

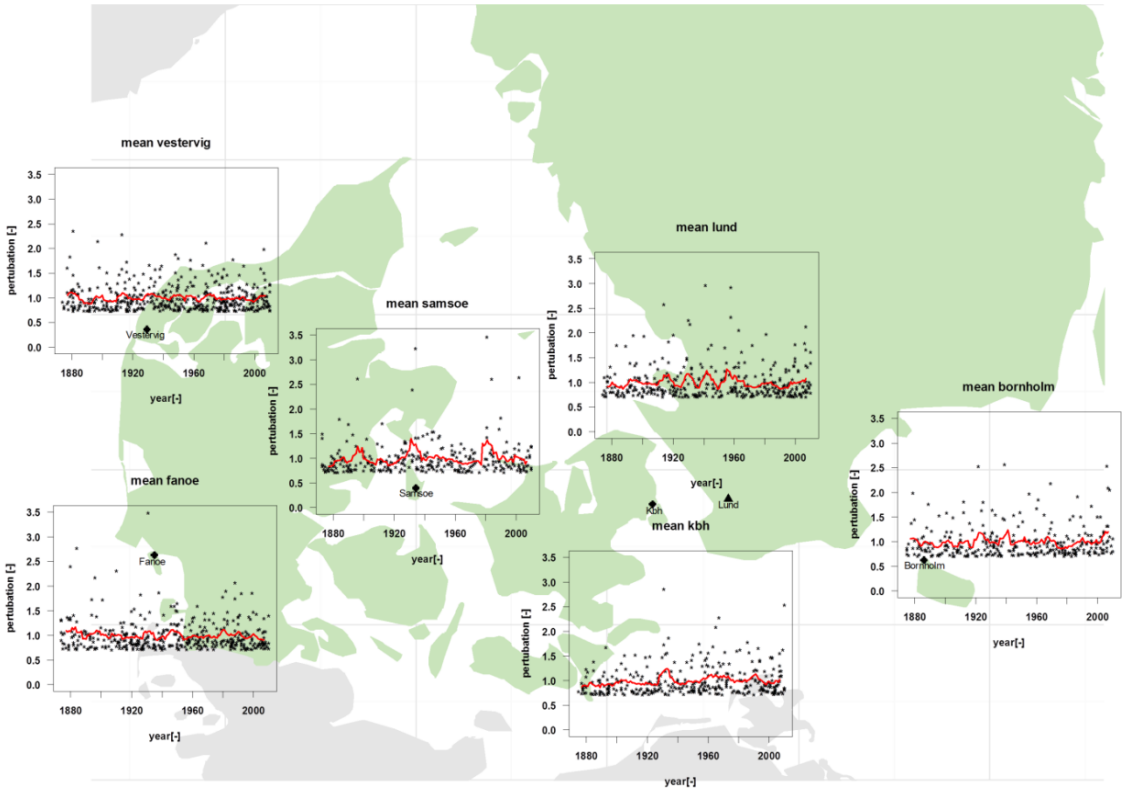

Figure 6: Annual variation of the mean magnitude of extreme events (black dots) and multidecadal variation of the smoothed series of μ (red lines) based on 137 years of measurements for six stations in Denmark and southern Sweden. The POT threshold is 19.2 mm/day and the window length is 7 years. The figure adapted from Gregersen *et al.* submitted a.

The spatial structure of the signal over Denmark could be random, but it may possibly be due to the fact that the west coast stations are dominated by changeable coastal weather. Gregersen *et al*. (submitted a) shows by comparison to the DMI dataset with 56 stations that the Eastern part of Denmark displays a more consistent signal, and that oscillations of the *pf* series for Kbh partly can be explained by an index derived from sea level pressure differences between Gibraltar and Haparanda. Apparently the general increase are driven by events in the spring and autumn, but Gregersen *et al*. (submitted a) did not find a large-scale driver for the increase. It could be caused by the increase in annual precipitation or the increase in global mean temperature. Alternatively, the general increase may also be interpreted as a natural variation.

The multidecadal variation of μ is shown in Figure 17 together with the year to year variation. Gregersen *et al*. (submitted a) show a zoom where the multidecadal variation appears more clearly. There is an indication of a pattern for Samsoe, but compared to the overall variability this has little practical implication. Finally, Figure 18 shows the variation of a 2-year event computed for the 13 independent 10-year time slices.

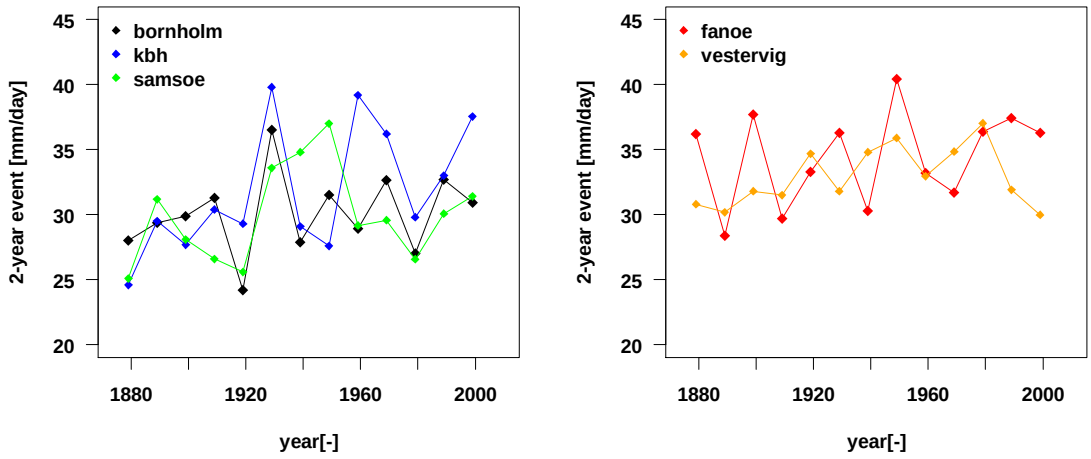

Figure 18: 2-year events for the five stations estimated from the 13 independent subseries with a length of 10 years.

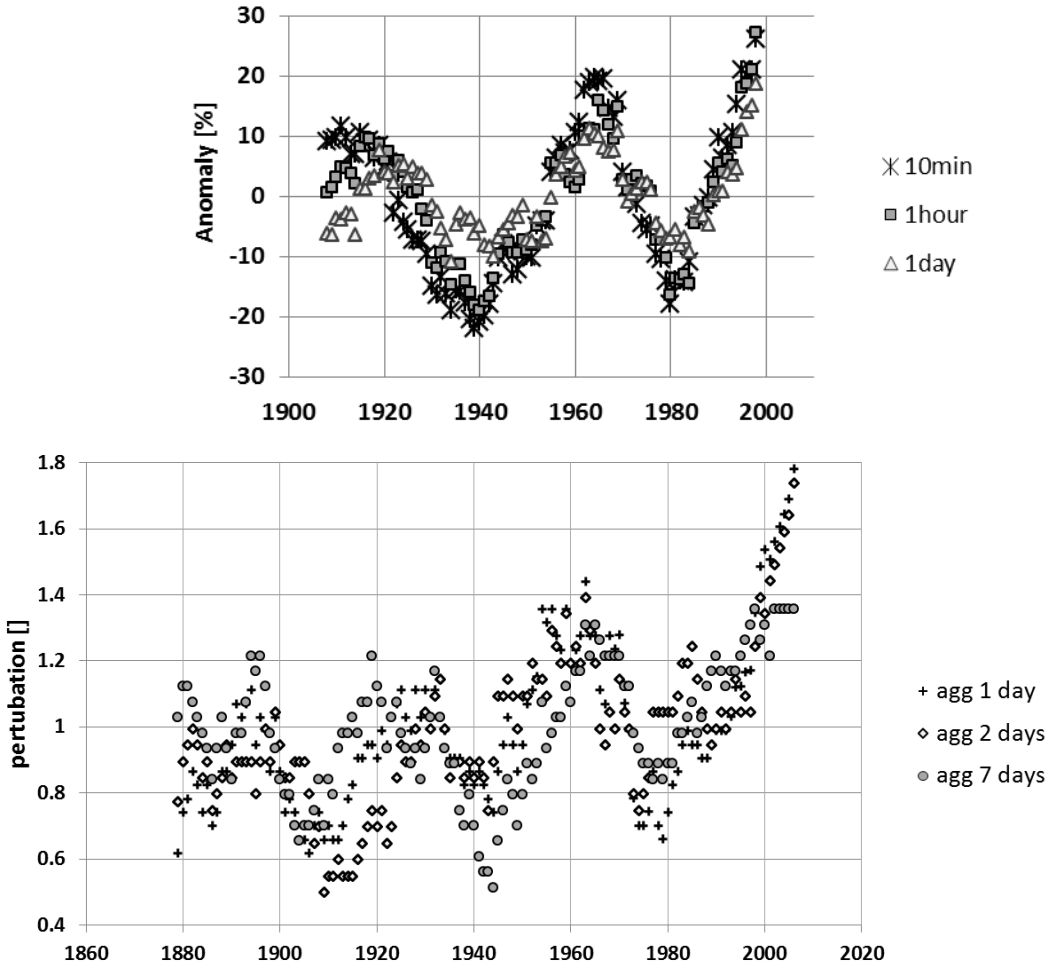

Figure 19: Multidecadal variation for different precipitation durations. Top figure is made by Willems (2013b) with data from the Uccle rain series for the average extreme quantile; the POT threshold corresponds to an average of three exceedances pr. year, in the JJA season, window length is 15 years. Bottom figure is for Kbh for the frequency of extremes; the POT threshold corresponds to an average of three exceedances pr. year in 1961-1990; window length is 10 years.

It is highly relevant to asses if the variations in λ found in the long smoothed daily series also exist for sub-daily rainfall. Using a long high-resolution series from Uccle, Belgium (Ntegeka and Willems 2008), it is found that the variations are consistent in smoothed series of precipitation durations between 10 min and 1 day. In

fact, is seems like the amplitude of the oscillations increase when the aggregation level decreases, see Figure 19 (top). Note that variation in the average quantile primarily is driven by variations in the frequency of the extreme events (Ntegeka and Willems 2008). Aggregations of the Kbh series, see Figure 19 (bottom), show similar tendencies for durations up to one week. However, for Vestervig (not shown) there is less consistency between the three analysed durations. This is assumed to be due to the coastal climate of the region. In summary, it seems reasonable to assume that the oscillating behaviour observed in smoothed series of daily extremes in Denmark can be transferred to lower precipitation duration. Hence, it is likely that the majority of the observed increase in λ in the SVK data can be attributed to natural variation rather than a direct response to human activity over the last 30 years. This is evident from Figure 20 that compares the increase in λ for the SVK station in Søborg with the multidecadal variations in λ for the smoothed long Kbh series.

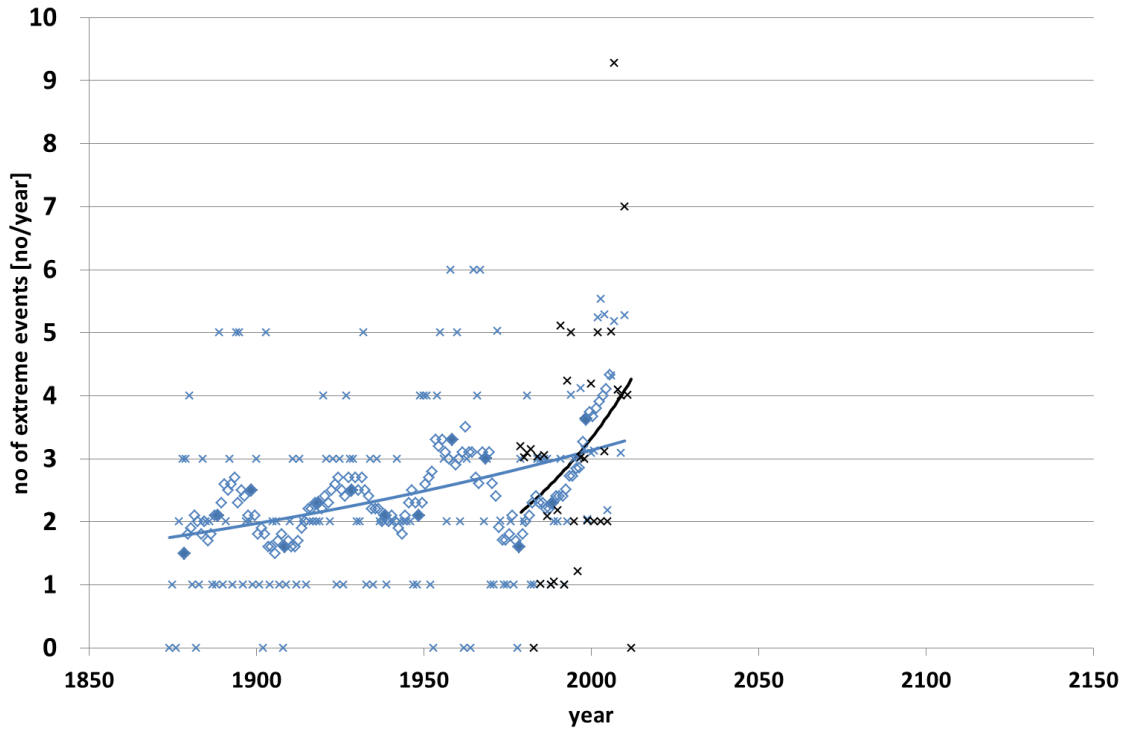

Figure 20: The observed increase in λ for accumulated daily rainfall for station 30222 in Søborg (black), compared to the multidecadal variation in λ for the long DMI series for Kbh (Blue). Crosses are annual number of extreme events, filled circles are the 13 independent points generated by a block average of 10 years, empty circles are the smoothed series and lines the modelled increase.

Finally, it is evaluated to which extent the trend in the SVK data affects the regional model. As shown in Figure 2, the number of station-years included in the regional model has increased during the recording period 1979-2012. In the first 12 years of the record (1979-1990) the number of station-years is relatively constant, around a level of 40 station-years per year, and then increases up to a level of about 70 station-years per year during the last 12 years (2001-2012). As discussed above, both λ (for all design variables considered) and μ (for some design variables) show an increase over the recording period 1979-2012. To investigate the sensitivity on the results of the number of station-years and increases in the λ and μ parameters, the regional model has been estimated using a sub-sample consisting of all stations with more than 30 years of data. This sub-sample includes 31 stations with a total of 999 station-years, evenly distributed over the recording period (see Figure 2).

The regional model estimated from the sub-sample gives smaller estimates of extreme intensities; up to 3% smaller for a 2-year return period, 5% for a 10-year return period, and 10% for a 100-year return period (see Figure 21). The differences between the two models are largest for durations up to 3 hours.

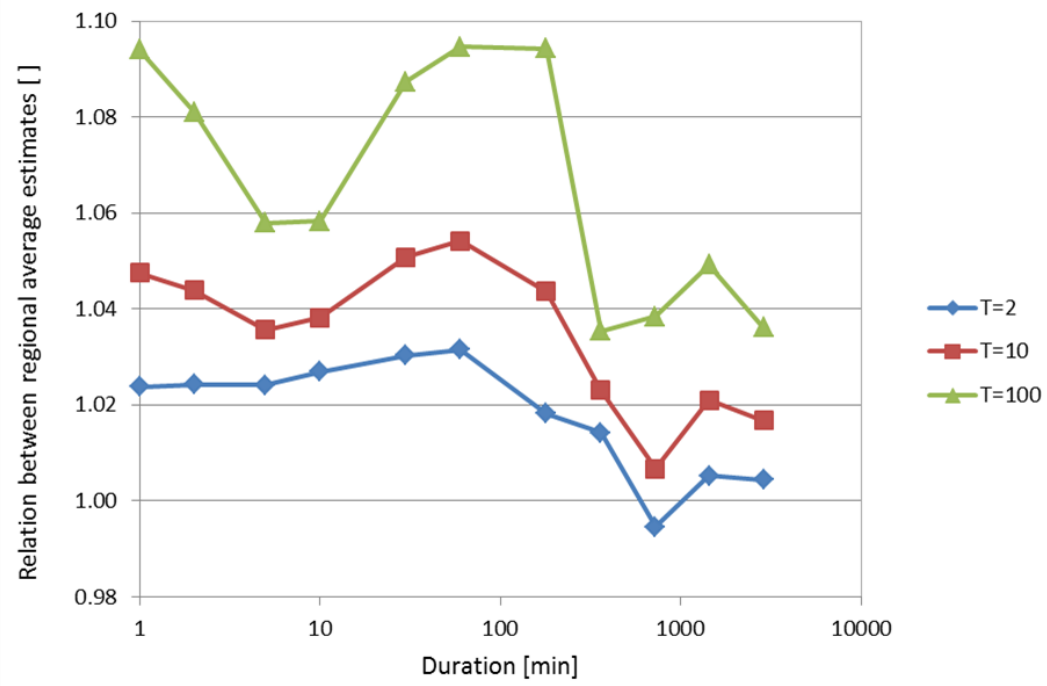

Figure 21: Relation between regional average estimates based on data from the full sample (83 stations) and the sub-sample (31 stations) for different durations and return periods T (years).

The uncertainties of the extreme intensities estimated from the regional model are smaller for the model based on the sub-sample. This is illustrated in Figure 22 for station 30451 (similar results are obtained for the other stations). The differences in uncertainties are largest for smaller durations and larger return periods. As shown in Figure 22, for 1-hour duration the uncertainty on the 2-year event estimate is about twofold for the model based on the full sample (relative standard deviation of 8.6%) compared to the model based on the sub-sample (4.4%), and larger differences are seen for the 100-year event estimate (23.7% and 9.1%, respectively). For the 24-hour duration the differences between the two models are smaller, e.g. 7.1% and 5.1% for the 2-year event estimate, and 16.7% and 9.2% for the 100-year event estimate.

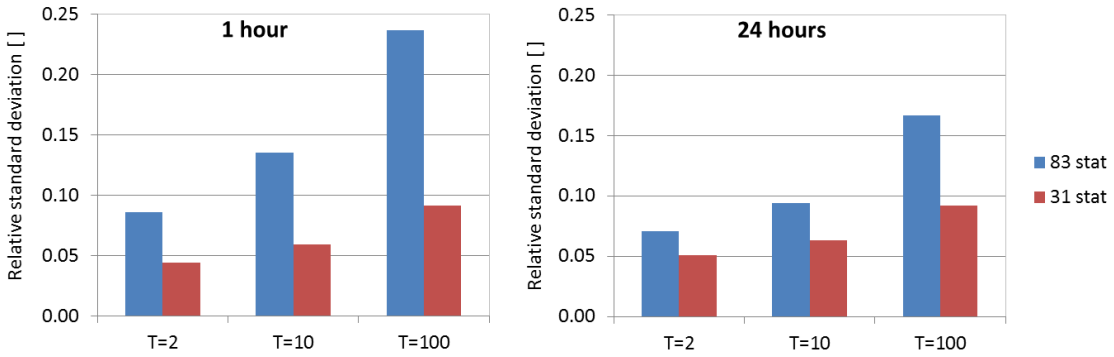

Figure 22: Relative standard deviation of intensity estimates at station 30451 for different return periods T (years) using the regional model based on data from the full sample (83 stations) and the sub-sample (31 stations) for 1-hour (left) and 24-hour (right) durations.

This analysis shows that the relatively larger contribution of station-years in recent years in the sample combined with increases in λ and μ gives larger estimates of extreme intensities as if only the records that cover the full observation period were included in the regional model. Thus, the regional model in Section 4.1 puts relatively more emphasis on recent data. However, a model based on a sub-sample of stations with full records will underestimate the uncertainty. The large uncertainty of the estimates from regional model in Section 4.1 reflects not only sampling uncertainty and spatial variability but also the temporal variability in the data. Since it is currently not possible to attribute the recent observed increases to anthropogenic changes or natural variability, the regional model using the full sample provides the best estimate according to current knowledge of extreme rainfall characteristics and associated uncertainties.

4.3 Stochastic weather generator and temporal disaggregation

The NSRP WG have been validated in several studies (Cowpertwait *et al.* 1996; Cowpertwait 1998; Burton *et al.* 2008; Burton *et al*. 2010) and no further validation is attempted here. Instead this section focuses on the results from the disaggregation approach. Figure 23a shows the scaling relationship for precipitation at one of the selected stations. The scaling relation is log-log linear in the chosen range of durations, and it differs from winter to summer. Figure 23b highlights the difference between winter and summer. It is seen that in the summer period the slope of the moments with an order higher than 1 is smaller than for winter, meaning that there is less difference between the precipitation characteristics at short and long durations in summer compared to winter. The difference between the two seasons increases with the order of moments. As the higher order moments are mostly influenced by the tail of the distribution, it can be concluded that the difference occur from the short duration summer extremes illustrating the effect of convective storms on the precipitation characteristics. For further details, see Sunyer *et al.* (in review a).

Figure 24 shows the validation of the model by comparing IDF-curves of the generated and observed rainfall series. The model has been run 10 times to illustrate the variability of the results. It is seen that the IDF-curves from the generated series have a slightly convex shape in a log-log plot compared to the linear IDF-curve for the observed rainfall series. The WG is calibrated on CGD and hence simulates areal rainfall, in which the extreme rainfall characteristics are not directly comparable to the SVK data. The cascade model is, however, calibrated on point rainfall, as no series of high-resolution gridded rainfall are available. This may introduce an error because the scaling properties of point rainfall and areal rainfall are not necessarily identical.

The range of climate factors obtained from this downscaling approach is presented in Section 4.5 and 4.6, while the synthetic rainfall series for future and present are further discussed in Section 4.7.

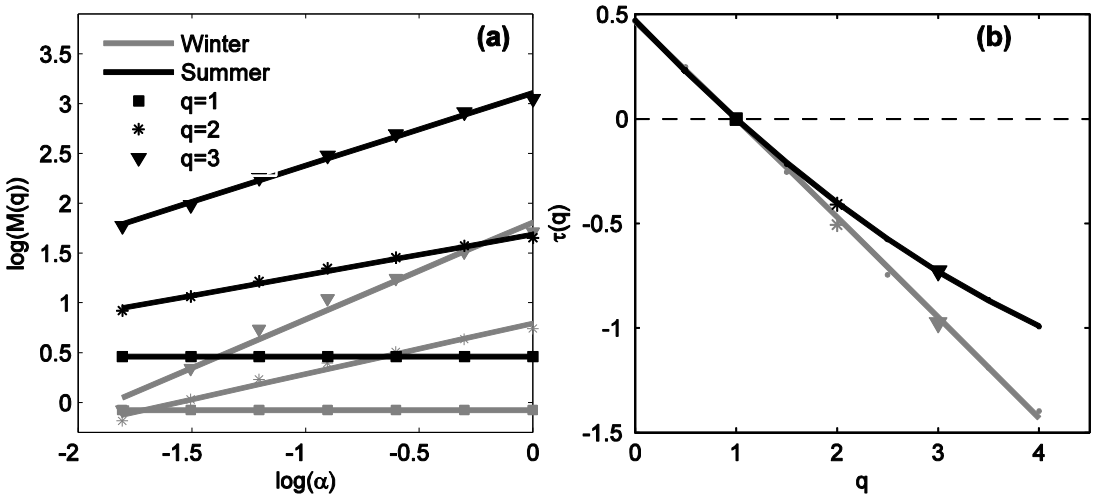

Figure 23: The scaling relationship for station 30131 applied in the estimation of the parameters for the random cascade model. *q* denotes the order of non-central moments. *α* represents the temporal resolution in the disaggregation cascade and a log(*α*) value of 0 and -1.8 correspond to 32 and 0.5 hours, respectively. *τ* denotes the inverse slope of the regression lines. The figure is adapted from Sunyer *et al*. (in review a).

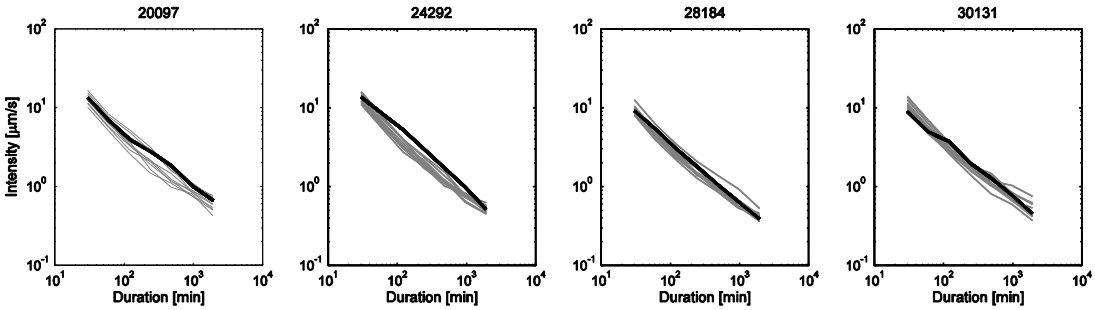

Figure 24: Validation of the random cascade model at four SVK stations, comparing the IDF-curves from 10 cascade model realisations with the IDF-curve from the observed series.

4.4 The climate analogue method

For the climate analogue method no explicit validation procedures is possible. The sensitivity of the result can however be indicated by means of applying different weights to the indices when calculating the metric and carrying out a split-sample test between different RCM simulations. The range of climate factors obtained from this downscaling approach is presented in Section 4.5.

A well-known limitation of the climate analogue method is that suitable analogue regions for the future climate might not exist. This situation could occur if climate change alters the fundamental mechanisms of the climate system. It is unknown at what global temperature level this will happen but Arnbjerg Nielsen *et al.* (submitted) shows that in the high-end 6° scenario it becomes difficult to identify suitable analogue regions. Using the A1B scenario suitable regions, however, can be found (Arnbjerg Nielsen *et al.* in prep.).

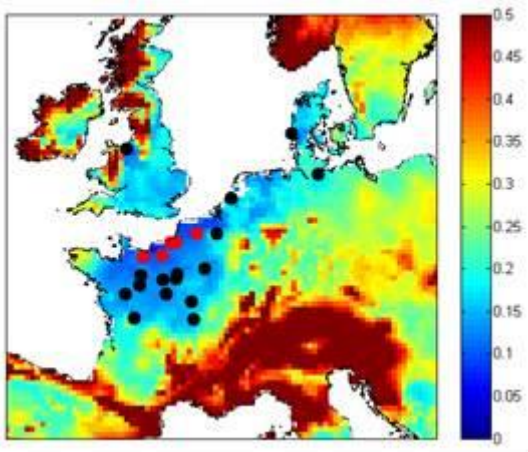

Figure 25: The metric for regions with can serve as analogues for the Danish climate in 2071-2100. The metric takes values close to 0 for regions which serve as good climate analogues. Dots indicate available information on design precipitation, red dots indicate the five selected stations.

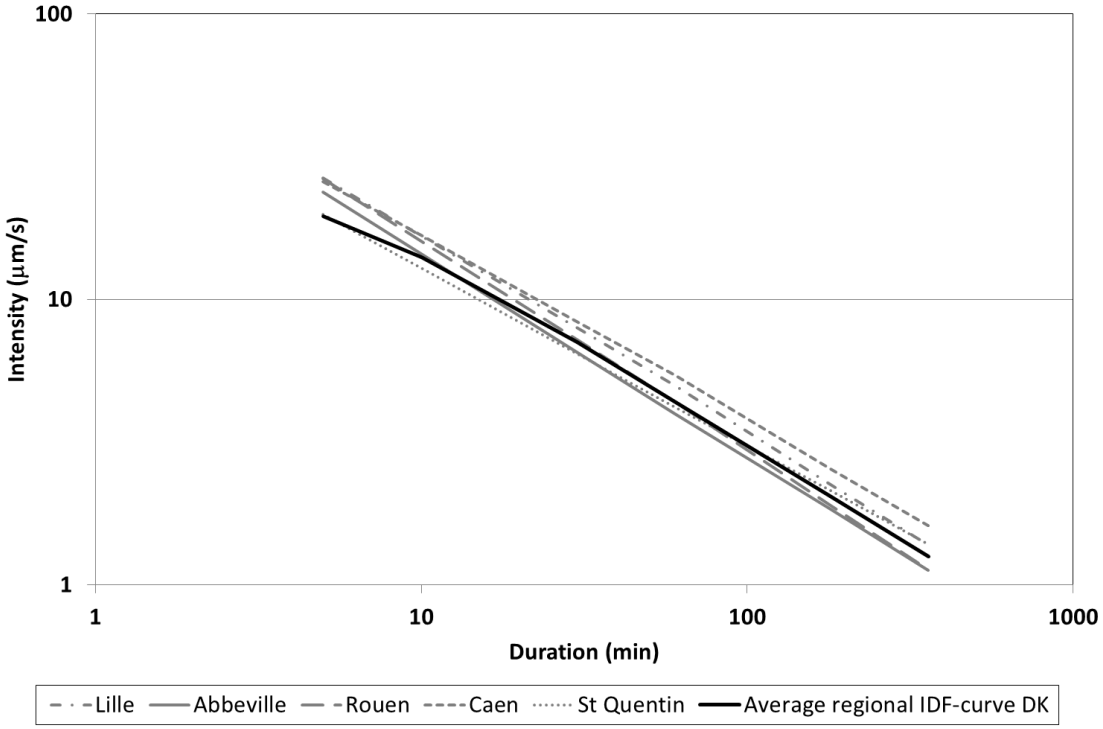

Figure 26: Obtained IDF curves for five French stations compared to the average regional IDF-curve for Denmark (see Figure 9) for a return period of 2 years

In this case the output from the climate analogue method is a map indicating which areas of Europe that can serve as good climate analogues for the future Danish climate, see Figure 25. The regions with the smallest metric are the northwest of France, Belgium, Netherlands, west coast of Denmark, and southeast of Britain. Compared to where information on design precipitation is available and the quality of the data, five stations in northwest of France is selected. The IDF curves for these stations are given in Figure 26 for a return period of 2 years, together with the regional IDF-curve for the present Danish climate, see section 4.1. It is seen that most, but not all, of the analogues indicate an increase of the design intensities. The sensitivity test indicates that the selected French gauges are robust estimates of the climate analogue. Given the large natural variation of precipitation extremes over time it is however a weakness that no information about the measurement period is available for the French data. In general the calculated climate factors are lower in this

study than reported in Arnbjerg-Nielsen (2012), primarily because of the estimates of the present Danish precipitation extremes has increases in the present study compared to the recommendation used in Arnbjerg-Nielsen (2012).

4.5 Climate factors 2071-2100

The different downscaling methods and the ensemble of RCMs lead to a range of different *CF* estimates, which needs to be compared. This section focuses on the far future 2071-2100. All methods use 1961-1990 as the present climate, leading to a projection period of approximately 100 years. However, the control period in the two high-end scenarios is different (see Table 3) leading to projection periods of less than 100 years. Still both sets of *CF*s are considered as projected changes for the far future and hence comparable to the *CF*s estimated in the present report.

In summary the downscaling methods and available additional datasets on high-end scenarios lead to the following CF estimates:

- **DC:** *CF*s from the delta change approach for extremes estimated directly from RCM output.
- **WG:** *CF*s from the delta change approach for extremes estimated from RCM output spatially downscaled by the WG
- **WG+Disagg:** *CF*s from the delta change approach for extremes estimated from RCM output spatially downscaled by the WG and temporally downscaled by the random cascade model
- **CA:** *CF*s from the climate analogue method
- **6 Deg:** *CF*s from the 6° scenario (Arnbjerg-Nielsen et al. submitted)
- **RCP:** *CF*s from the two RCP scenarios (Arnbjerg-Nielsen et al. submitted, Sørup et al. in prep.)

In Figure 27 the notation of the precipitation duration given in front of the downscaling method or dataset indicates the temporal resolution of the applied RCM data.

Sunyer *et al.* (in review a) concludes that there is a robust indication of an increase of the extreme precipitation, across the ensembles and across all the applied downscaling methods. For a duration of one hour the smallest variance both between the different RCMs and across Denmark is obtained when the RCM output is spatially downscaled by the WG and temporally downscaled by the random cascade model. The two RCMs having available precipitation output at a temporal resolution of 1 hour, both lies in the upper end of the ensembles. It was furthermore found that for RACMO there is a small disagreement between the *CF* estimated from 1 hour max and 1 hour (Sunyer *et al*. in review a). The two models are therefore not included in the final determination of *CF*s for use in urban drainage design. Regarding the spatial variation of the *CF* over Denmark there is partly an agreement between the downscaling methods, but a high variation between the RCMs with respect to the spatial pattern of climate change (Sunyer *et al.* in review a). Hence, regionally distributed *CF*s cannot be justified and the results given below are factors spatially averaged over Denmark.

A comparison of the results from all methods and datasets are given in Figure 27. The estimated uncertainty is expressed as 68% confidence bands. With the available information it is possible to select a set of 'standard' *CF*s, which represents the most robust estimate of the expected future change and to reflect the uncertainty of the estimate by and additional set of 'high' *CF*s that reflects the upper 84%-quantile.

The first conclusion from the figure is that the currently used *CF* lies within the uncertainty limits of the new *CF* estimates. However, the mean of any of the three downscaling methods is below the current recommendations. The scenario which forced the ENSEMBLES simulations (A1B) represents less intense greenhouse gas emissions than the A2 scenario over a 100 year projection horizon. The found difference may reflect the relation between emission scenario and *CF*. The difference between the two RCP simulations supports this hypothesis. RCP8.5 can roughly be translated to the A2, while RCP4.5 has a trajectory close to B1, see sec-

tion 2.7. As the actual emissions since 2000 have been slightly higher than anticipated in the A2 scenario (Peters *et al.*, 2013), it seems reasonable to account for the scenario uncertainty by using the difference between the RCP 4.5 and RCP 8.5 to perturb the ENSEMBLES mean. A similar exercise can be done for the 6° scenario, where the relative difference between 1h max 6 Deg (orange dot) and 1h max RCP 4.5 (yellow dot) is even larger.

The results indicate that the *CF* depends on the duration, 1 hour being higher than 24 hours. The difference is, however, only judged to be of significance for the high-end scenarios. For simplicity the recommendation on mean *CF* values in relation to generation of design rain storms is still constant for all precipitation durations as a time-varying climate factor is difficult to implement in design recommendations using design storms.

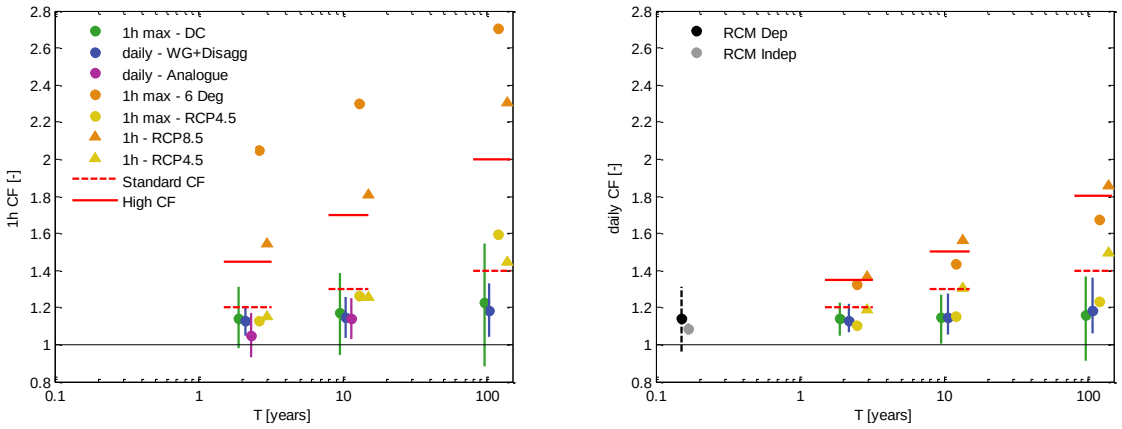

Figure 27: The estimated *CF* for 1 hour (left) and daily (right). They represent the relative change between the baseline period and the projection period 2071-2100. The dot indicates the mean *CF* and the vertical lines indicate the 68% confidence interval. Each high-end scenario (orange symbols) is paired with a RCP4.5 scenario (yellow symbols), the relative difference between the two shows the effect of the high-end scenario. The punctured red line indicates the currently used climate factors, while the solid red lines gives a subjective estimate of the 84% quantile of the *CF* taking all discussed sources of uncertainty into account.

A study by Sunyer *et al.* (in review b) concludes that ensemble averages for evaluation of future precipitation extremes should be corrected for 1) an underestimation of the uncertainty as the climate models are not independent, and 2) a bias in the mean as the error of the climate models change over the simulation period. The results from Sunyer *et al.* (in review b) are included in the figure to illustrate the effect of the two issues mentioned above. All calculated *CF*s in the current study assume independent models and constant bias, and hence underestimate both the upper confidence limit and the ensemble mean. This is (in a subjective way) taken into account when the *CF* values are selected.
The recommended *CF*s are given in Table 5

Table 5: Final *CF* based on three statistical downscaling methods, 18 climate model simulations and 4 emission pathways. The 1 hour values can be used as a replacement for guideline no. 29 (WPC 2008), 1 day values are only used for selection of the two future time series

	1 hour		**daily**	
	Standard	High	Standard	High
0.2-year event	-	-	1.18	1.25
2-year event	1.2	1.45	1.2	1.35
10-year event	1.3	1.7	1.3	1.5
100-year event	1.4	2	1.4	1.8

4.6 Climate factors for the near future

*CF*s for projection periods of less than 100 years can be required in some situations. There are several methods for obtaining these:

1) Extrapolating the pattern of natural variations on the basic of the power spectrum as briefly discussed in Section 4.2
2) Directly from the climate model simulations, following the procedures of Section 3.4-3.6 but using another scenario period than 2071-2100
3) Downgrading the *CF* for 2071-2100 assuming that the *CF* depends linearly on the length of the projection period as recommended by WPC (2008).

It is assumed that with a shorter projection horizon the relative influence of the natural variation in comparison to the projected mean effect of climate change will increase. However, it is difficult to statistically justify an extrapolation of the pattern observed from 1874 to present. It has been shown that the natural variation is partly driven by large scale variation in Sea Level Pressure (SLP) over the North Atlantic (Gregersen *et al.* submitted a), making the pattern more robust, but there is no guarantee that the oscillations will continue with the same period and amplitude. Hence method 1 is not attempted here. Future research could explore if SLP projections can be extracted from GCMs/RCMs and used as the basis in the projection of future rainfall extremes, but this is outside the scope of the present project. Any future projections of the variations in λ should be based on the full spectrum as discussed by Lee and Ouarda (2010).

In the PRUDENCE project (Christensen and Christensen 2007) to which the climate model simulation used by WPC (2008) belongs, the model communities agreed to run simulations for two thirty-year long time slices, being 1961-1990 and 2071-2100. The difference between the two periods was meant to represent the relative changes in the climate due to anthropogenic greenhouse gas emissions over a projection period of 100 years, even though the actual timespan between the two periods represents 110 years. Hence the climate factors by WPC (2008) also represent a projection period of 100 years, which conveniently corresponds to the projected lifetime of many urban infrastructures. The period 1961-1990 is defined by WMO as the current 'climate normal period' and will remain so until 30 additional years of observation is available (1991-2020). When the ENSEMBLES project (van der Linden *et al.* 2009) was initiated, the increased computational capabilities allowed for transient simulations covering the entire period from 1950 to 2100. This allows for calculations of climate factors with shorter projection periods. However, we are challenged by the fact that the climate of today already is assumed to be affected by the past greenhouse gas emissions and that the period 1961-1990, hence, represents a different climate than the present. Still, it is assumed that the relative change remains the same. Another limitation of the short projection periods is that the natural variation might be of greater relative importance than the GHG forcing, as mentioned above. With all the mentioned limitations in mind this project still provides *CF*s for the near future. These are calculated for the periods 2021-2050 and 2041-2070, relative to 1961-1990 and therefore represent a projection period of 50 (near future) and 70 years (middle future), respectively, even though the actual start dates of the scenario periods is less than ten and thirty years into the future counting from 2014.

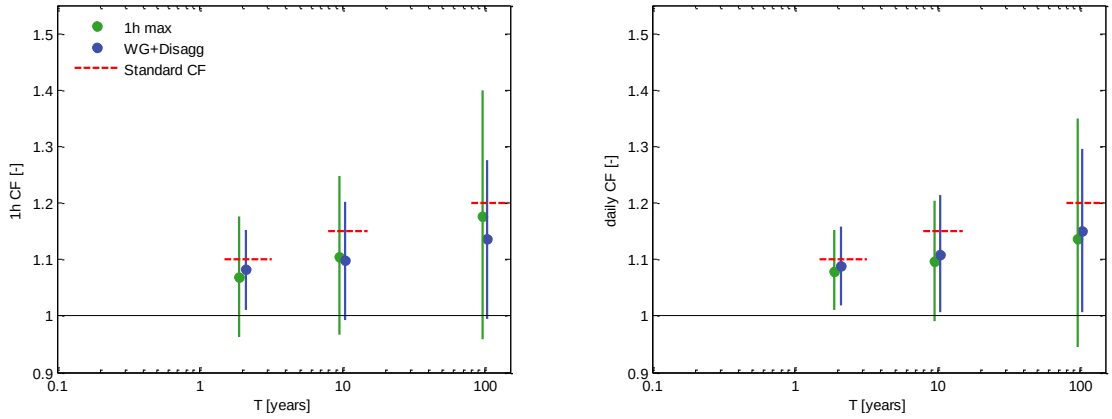

Figure 28: The estimated *CF* for 1 hour (left) and 24 hours (right) using a projection period of 50 years. The dot indicates the mean *CF* and the lines indicate the 68% confidence interval. The punctured red line indicates the currently used climate factors.

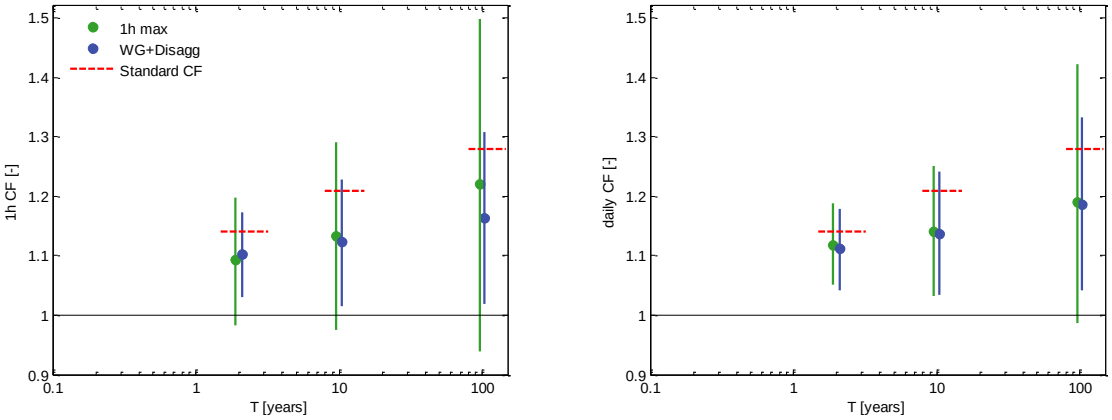

Figure 29: The estimated *CF* for 1 hour (left) and 24 hours (right) using a projection period of 70 years. The dot indicates the mean *CF* and the lines indicate the 68% confidence interval. The punctured red line indicates the currently used climate factors.

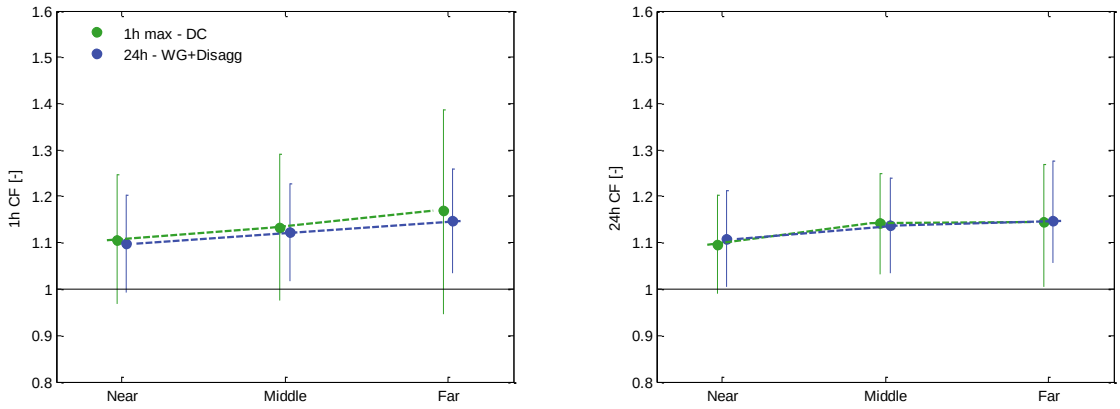

Figure 30: The *CF* as a function of the projection period, estimated from two different downscaling methods and for two precipitation durations (left: 1 hour, right: 24 hours) for a return period of 10 years. Vertical lines are the 68% confidence intervals based on the ensemble of climate model simulations. Stipulated horizontal lines indicate the change of the *CF* with the projection period

The *CF*s obtained from method 2 and 3 are given in Figure 28 and Figure 29. It is seen that the two methods give very similar results. The *CF*s obtained from method 2, are slightly higher only because the *CF*s from which they are interpolated (see Table 5) are higher than the ensemble mean as discussed in Section 4.5. By plotting the increase of the *CF* as a function of the projection period the linear relation is confirmed, see Figure 30. In summary, recommended *CF*s for projection periods of 50 and 70 years, respectively, are given in Figure 30 and Table 7. These are based on a linear reduction of the *CF*s in Table 5 according to the reduction in the projection period.

Table 6: *CF* for a projection period of 50 years

	1 hour		**daily**	
	Mean	High	Mean	High
2-year event	1.10	1.23	1.10	1.18
10-year event	1.15	1.35	1.15	1.25
100-year event	1.20	1.50	1.20	1.40

Table 7: *CF* for a projection period of 70 years

	1 hour		**daily**	
	Mean	High	Mean	High
2-year event	1.14	1.32	1.14	1.25
10-year event	1.21	1.49	1.21	1.35
100-year event	1.28	1.70	1.28	1.56

4.7 Synthetic precipitation series for the future conditions

To provide simulated high-resolution precipitation series for future conditions, the two disaggregated WG series, which best reflect the future conditions represented by the set of mean and high climate factors, are selected, together with a series for the present, as represented by the regional model over Denmark, see Section 4.1. The following selection procedure is applied:

1. A regional IDF-curve from Figure 9 is applied as a representation of present design precipitation over Denmark.
2. For the 2, 10 and 100 years return period, the values corresponding to 1 hour, 6 hours and 1 day from the regional IDF for the present period are multiplied by the *CF*s to obtain the values for the future climate. Section 4.5 only provides *CF*s for precipitation durations of 1 hour and 1 day, an average of the two is used as *CF* for 6 hours.
3. For each of the disaggregated WG series:
    - Estimate the hourly, 6 hourly and daily T-year events for the 2, 10 and 100 years
    - For the three return periods, estimate the Root-Mean-Squared-Error (RMSE) between these values and the values for the present/future estimated in (2).
    - Calculate the average of the RMSE estimated for each of the return periods
4. Select the time series with the minimum RMSE

The IDFs of the three selected series are shown in Figure 31, together with the nine points from which they are chosen and overall variability of the simulated series.

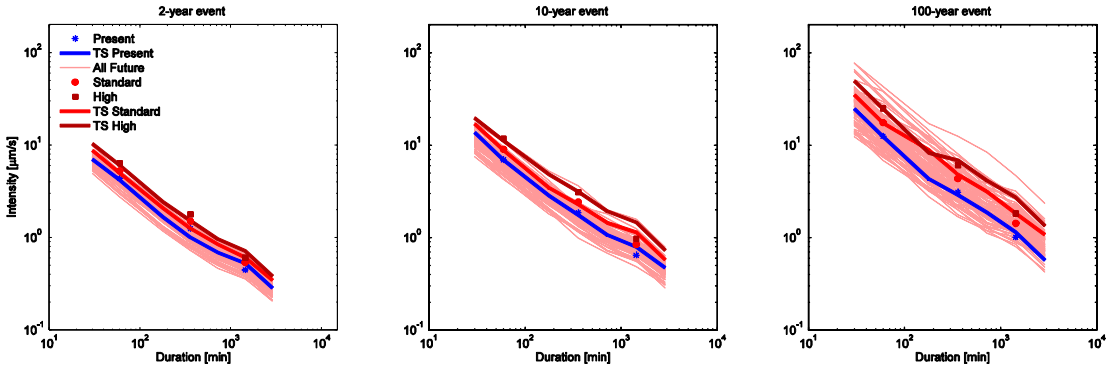

Figure 31: IDF curves for simulated precipitation series (light red). The thick blue line is the present average IDF curve for Denmark. The red and dark red dots are the future T-year events corresponding to the mean and high *CF*, respectively. The thick red and dark red lines are the IDF curves for the time series, which gave the optimal fit to all selection criteria

The precipitation statistics for the three series are given in Table 8, while Figure 32 shows the seasonal variations. In general all indices correspond well to the known and expected future variation of precipitation.

Table 8: Annual precipitation statistics for the three simulated precipitation series

	Present	Mean scenario	High Scenario
Mean annual precipitation [mm/year]	729	844	729
Interannual variation (sd.dev.) [mm/year]	98	136	118

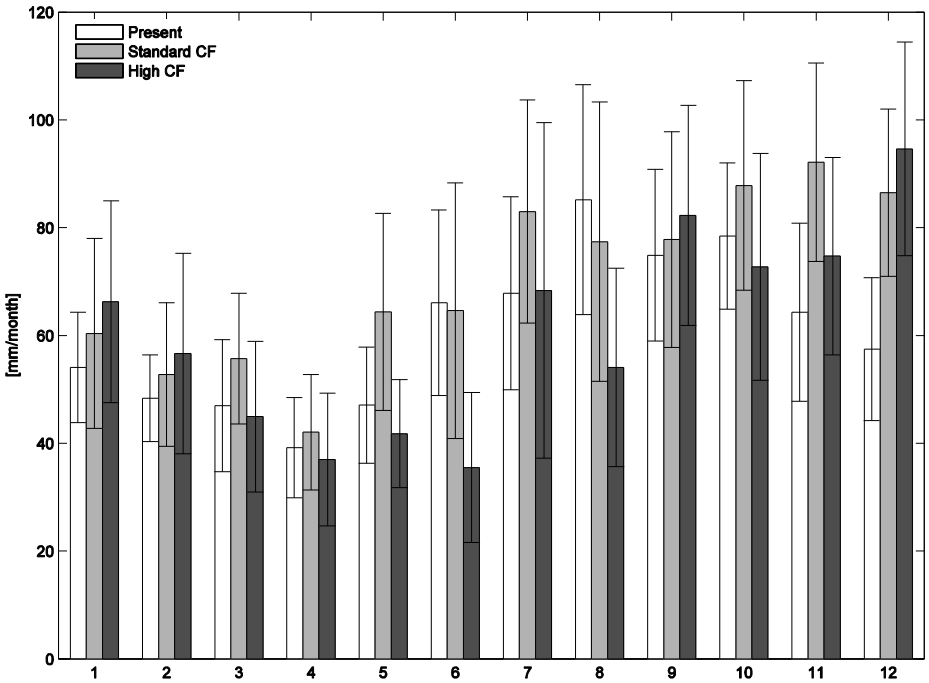

Figure 32: Monthly precipitation statistics for the three simulated precipitation series.

In Figure 31 it is noted that for a return period of 2 years the IDF curves for the simulated series tend towards a convex shape rather than the concave shape expected in observational data. The problem seems worse than concluded when the approach was validated in Section 4.3. This makes it challenging to find an IDF curve (representing the present climate) that lies within the bounds given by the variability over Denmark for

all durations, see Figure 33. Paludan *et al.* (2014) find that the disaggregation is very disrupt, leading to several sub-hourly design events on the same day. The problematic behaviour could be due to a limitation of the random cascade model itself, but it could also be due to the fact that the climate change impact is assessed on a series that is smoothed by spatial and temporal averaging while the series used to estimate the disaggregation is discontinuous because of the properties of the tipping bucket. The problem is discussed further in Section 5.3.

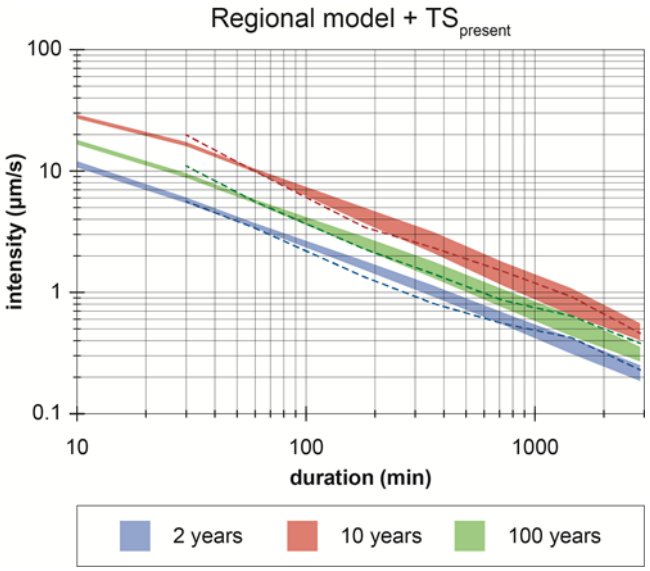

Figure 33: IDF curves for synthetic precipitation series representing the present compared to variability over Denmark given by the regional model, see Figure 9. Blue is 2 year, green 10-year and red 100-year return period. Coloured areas are representing regional model. Stipulated lines are representing the synthetic precipitation series.

5. Discussion

This section discusses the interpretation and implication of the found natural variation. Also the actual impact of the new guidelines in comparison to the current practices is addressed, both in general and by using the municipalities of Århus and Greve as examples. Finally, the application of the generated synthetic rainfall series is discussed.

5.1 Implications of the trend and the natural variation compared to climate change

In Section 4.2 it was shown that λ has increased significantly for all analysed precipitation variables during the 34 years where the SVK network has been active. However, in the same section it was concluded that a smoothed λ series exhibits an oscillatory variation. Gregersen *et al.* (submitted a) points to the fact that the most recent oscillation high in the smoothed Kbh series appears larger and more persistent than its predecessors, see Figure 34 (top). Although this hypothesis cannot be tested with the data currently available, it might be interpreted as a sign of anthropogenic climate change. Still it can be concluded that the majority of the observed increase in the SVK data most likely is due to natural variation rather than impact of human activity over the last 30 years. In this section we address how the natural variation has affected urban design values over time and how the magnitude of the variation compares to the excepted effect of anthropogenic climate change.

The Danish design practices for urban drainage have changed significantly since the very first guidelines were published by the WPC in the early 1950's. This fluctuation over time has never been seen as an indication of non-stationary precipitation mechanisms. It is interesting to see to which extent *pf* defined in Section 3.3 is correlated to the variations in the recommended design intensities. The analysis focuses on Greater Copenhagen area, where the oscillation signal is strongest and, as mentioned earlier, partly correlated to an index derived from sea level pressure over the North Atlantic.

The result is given in Table 9 and Figure 34 include the following WPC guidelines

(1) **1950-1953** Design values for the four major Danish cities (WPC 1950 and 1953)
(2) **1974** Update of (1) with additional years of measurements (WPC 1974).
(3) **1999** Regional model for extreme precipitation based on data from the SVK network (WPC 1999)
(4) **2006** Updated regional model for extreme precipitation (WPC 2006)
(5) **2014** Updated regional model for extreme precipitation, see Section 4.1

(1) and (2) both have information from a pluviometer placed in Gentofte, while the location of a tipping bucket rain gauge in Søborg (station no 30222, 721023E 6181403N) is applied in the three different regional models (3)-(5), together with the at-site observations. The at-site design intensity for Søborg is estimated empirically from the series of observed precipitation. *pf* values are estimated from the Kbh series and a value above/below 1 indicates phases of high/low number of extremes (in the smoothed series). All design values from the guidelines are for a rainfall duration of 10 minutes, whereas all *pf* values are for accumulated daily rainfall. The variation in this variable is assumed to be valid for lower durations as well, see Section 4.2.

Table 9 and Figure 34 shows that the variation in the design values to some degree follow the pattern of the natural variation. However, the variation has not dominated the past design practice as 'Landsregnrækken' from WPC (1974), often was used for design instead of the local rain gauge estimates. 'Landsregnrækken' is significantly higher than the local estimate for Gentofte (see Figure 34) as several large events were measured in Århus during the specific observation period.

Table 9: Variations of 2-year event for a precipitation duration of 10 min for the Greater Copenhagen area compared to the perturbation factors representing the natural variation. The numbers given in parenthesis refers to the list of WPC guidelines given above. pf is estimated from the Kbh oscillation curve given in Figure 20, until 2005, and no value is given if the observation period extends this year . The at-site design intensity is estimated empirically from the series of observed precipitation.

	Design intensity [µm/s]	Observation period	Average *pf* during the observation period
Design value, Gentofte (1)	11.5	1933-1947	0.88
Design value, Gentofte (2)	12.2	1933-1962	1.03
Regional model, MAP 643 mm, Region Kbh West (3)	12.2	1979-1996	0.95
Regional model, MAP 643 mm, Region East (4)	13.0	1979-2005	1.13
Regional model, MAP 643 mm, CGD mean 27.4 mm/day (5)	13.9	1979-2012	-
At-site observations Søborg Waterworks	10.3	1979-1995	0.93
At-site observations Søborg Waterworks	15.7	1996-2012	-

The relative difference between the first estimate from 1933-1947 and the most recent estimate from the current version of the regional model is 1.2, while the relative difference between at-site estimates based on the first half of the observations from Søborg versus the last half is 1.5. This shows that the natural variation is highly important compared to the expected climate change impacts and that the period of observation has an impact on the estimated design intensities. As neither the general increase, nor the fluctuation of periods with high/low number of extreme events, are fully understood, the regional model using the full sample reflecting the natural variability provides the best estimate of design intensities according to current knowledge (see discussion of results in Section 4.2). However, the period of observation is relevant when applying historical time series for the analysis. A framework for comparing series of at-site observations with the regional model and potentially correcting historical time series was developed by WPC (1999), which can be used to correct short series of observations that do not represent the full range of natural variation.

Neither the general increase nor the fluctuations are directly accounted for in the *CF* estimates. Therefore, it is of key importance to understand how the natural variation and the anthropogenic climate change interrelates and thereby how to superimpose the changes caused by human activity onto the natural processes. The question is if the effect of anthropogenic climate change can just be added on top of natural variation that we see today (as the current framework assumes), if the interrelation will be in the form of amplification of the natural cycle, or if there will be even more complex interactions between the processes. Future research will pursue this question.

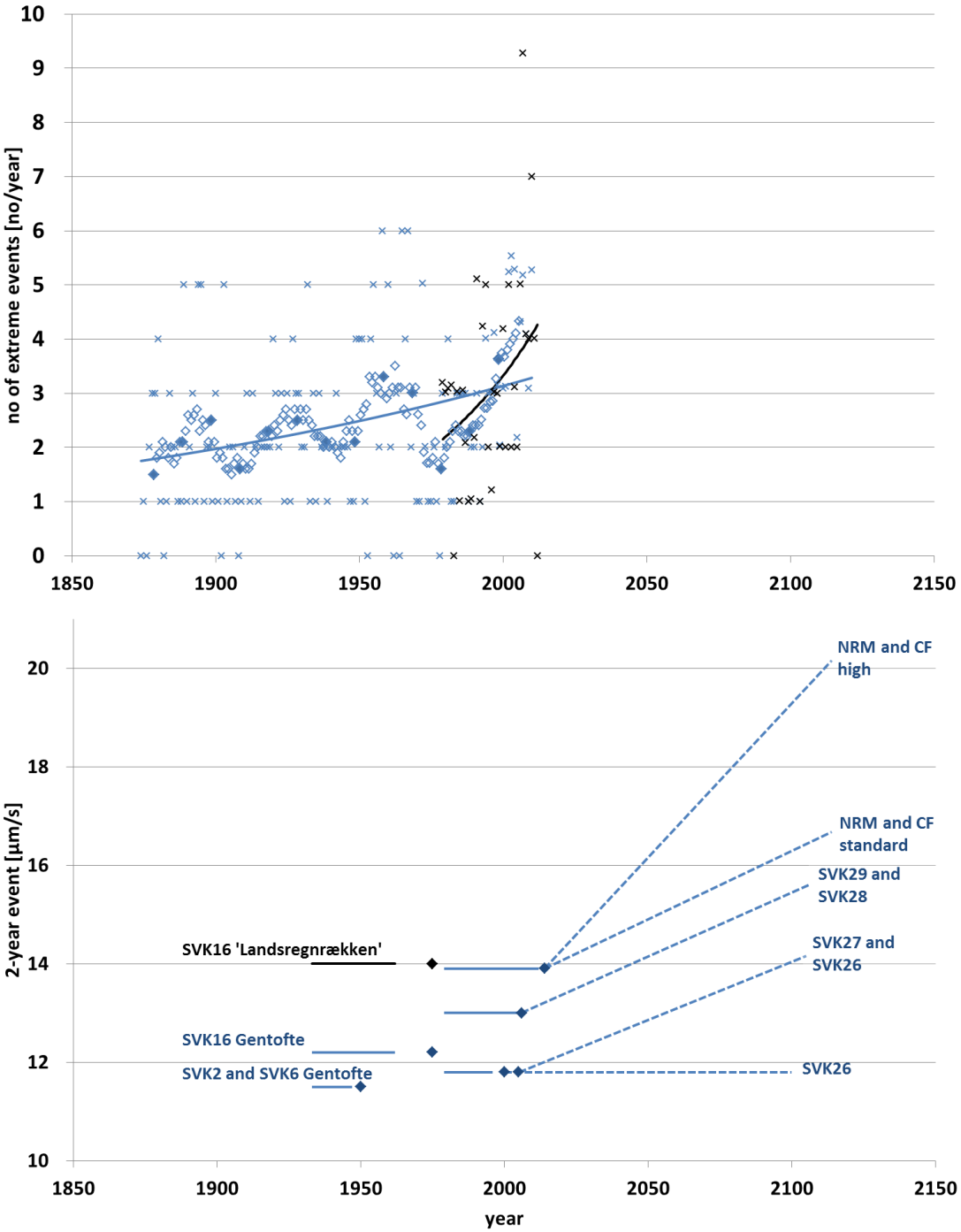

Figure 34: Top: The observed increase in λ for accumulated daily rainfall for station 30222 in Søborg (black), compared to the multidecadal variation in λ for the long DMI series for Kbh (Blue). Crosses are annual number of extreme events, filled circles are the 13 independent points generated by a block average of 10 years, empty circles are the smoothed series and lines the modelled increase. Bottom: Past, present and projected values for a 2-year event with a duration of 10 minutes given by the five major WPC guidelines on design intensities. Circles represent the publication year of the guideline, solid lines represent the years of measurements using to estimate the design intensities and punctured lines represent the projected future values. NRM denotes the new regional model.

5.2 Comparison with the regional model in guideline no. 28

This section addresses how design intensities from the new regional model (see Section 4.1) compares to guideline no. 28 (WPC 2006).

The differences between estimates based on the guideline no. 28 and the new regional model are shown in Figure 35 and Figure 36 for 1-hour and 24-hour intensities.

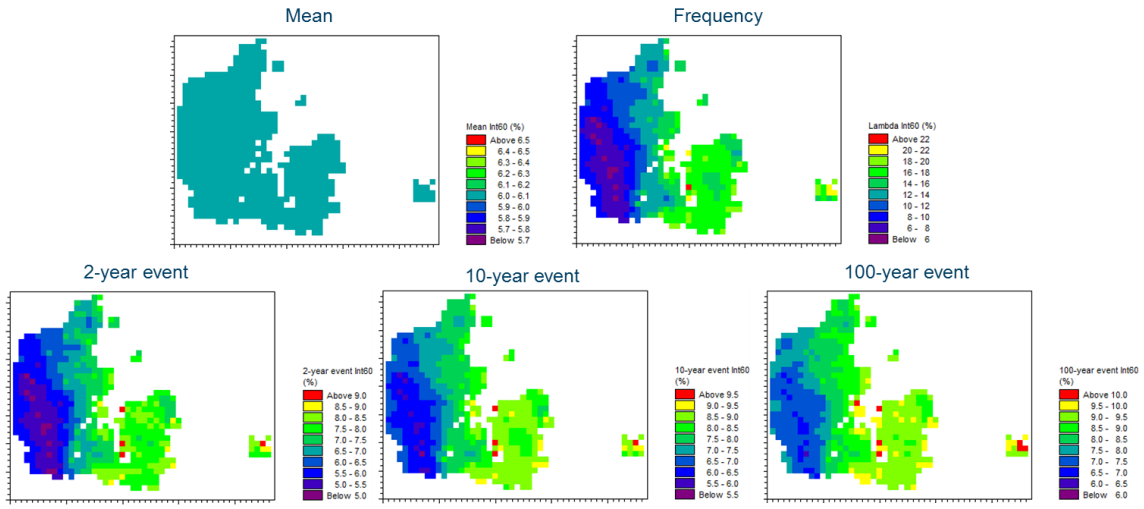

Figure 35: Differences in [%] between estimates based on the regional model in guideline no. 28 and the new regional model for 1-hour intensity: mean intensity (top left), average annual number of extremes (top right), and 2, 10 and 100-year events (bottom row).

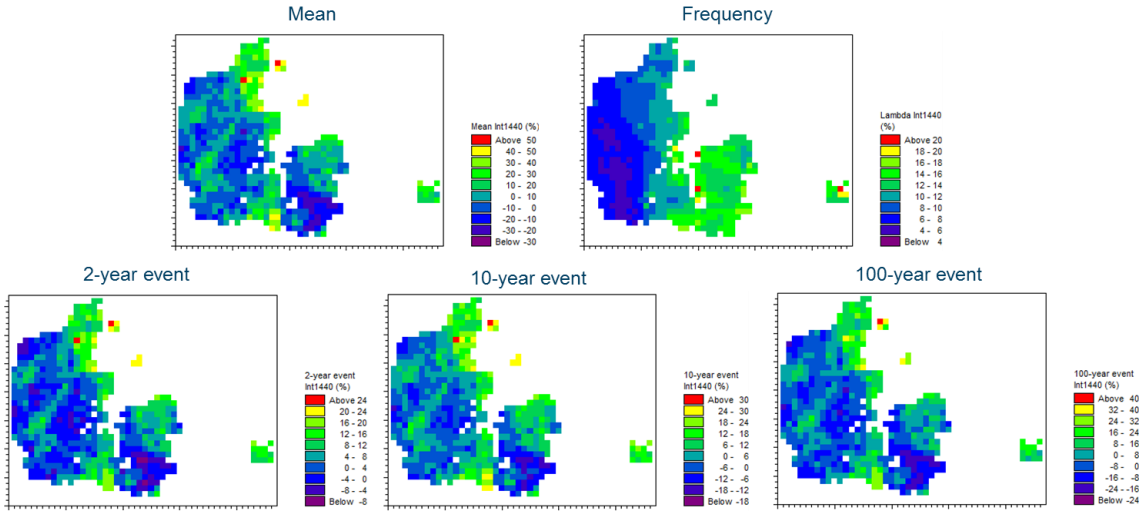

Figure 36: As in Figure 35 but for 24-hour intensity.

For the 1-hour intensity there is an increase in the mean intensity of about 6%, which is constant over Denmark, since both regional models have a regionally constant mean intensity. For the 24-hour intensity the change in mean intensity varies from -30% to 60%, with a regional pattern similar to the mean daily extreme of the DMI climate grid (Figure 9, top right). For both durations there is an increase in the average annual number of extremes, with an increasing pattern from west (from 4%) to east (up to 22%). For the 1-hour intensity, the changes in the extreme intensities follow the west-east pattern of the changes in the average annual number of extremes with an increase of 5-10% for the 2, 10 and 100-year return periods. For the 24-hour intensity, the changes in the extreme intensities follow the pattern of the changes in the mean intensity.

There are both decreases and increases; from -9% to 26% for the 2-year event, -16% to 36% for the 10-year event, and -30% to 59% for the 100-year event. Main increases are seen in the northern part of Jutland, north-east Sealand, southern islands and Bornholm. The range of changes between guideline no. 28, and the new regional model for the IDF curves are shown in Figure 37 for the 2, 10 and 100-year return periods. These ranges are calculated for the different durations as the minimum and maximum of the CGD gridded changes as shown in Figure 35 and Figure 36. For durations up to 1 hour there is a general increase of up to 10%, with only minor differences between the three return periods. For larger durations, both decreases and increases are seen with larger differences for increasing return period.

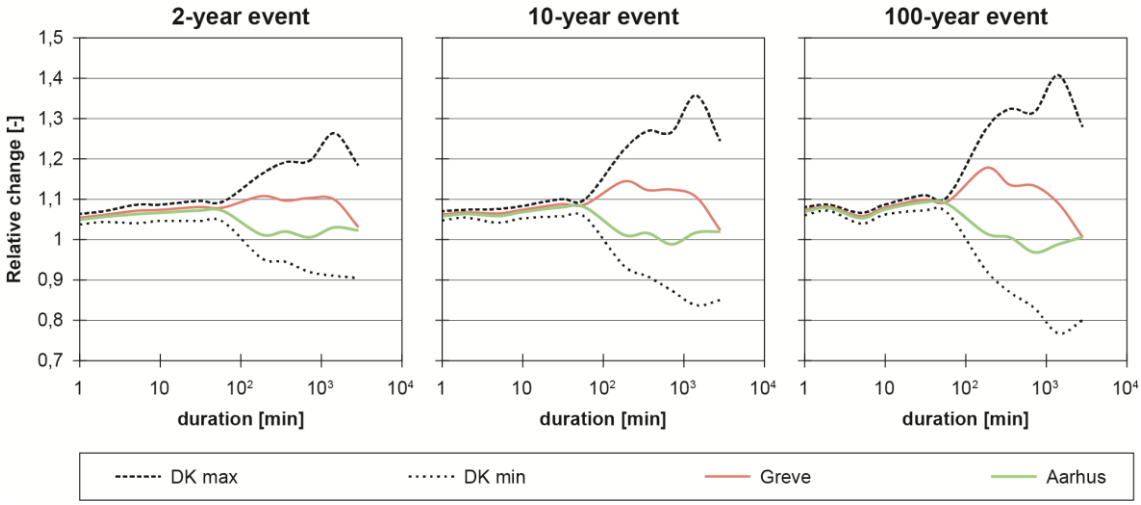

Figure 37: Relative change between SVK28 and the new regional model for a 2, 10 and 100 year event. The stipulated curves illustrates the variability over Denmark given by the CGD, while the red, blue and green curves show the change for Greve, Ålborg and Århus, respectively.

5.3 Evaluation of the synthetic precipitation series

The two high-resolution precipitation series for future conditions are supposed to be valuable in model simulations, where historical precipitation series currently are used. As regionally varying climate factors cannot be supported (see Section 4.5), the selected series represents all of Denmark, even though the present design precipitation varies over the country. To evaluate the possible implications of not having regionally different series for the future conditions, a precipitation series, which represent the present, is also selected by similar methods but using a *CF* of one (see Section 4.7). This series is compared to the at-site information from Greve and Århus, estimated from the local rain gauges that currently provide the precipitation series for the two sites, see Figure 38. Note that the figure only can be used to compare the properties of the synthetic series to at-site variability, IDF-curves for design purposes should be estimated from the regional model, not at-site information.

It is seen that the IDF curve for the simulated rain series falls outside the 68% confidence bands for a return period of 2 years; this is due to the convex behaviour of the IDF curves generated by the weather generator, as discussed in Section 4.3. For 10 and 100 years the design precipitation of a duration of 30 min is overestimated. Apart from this the IDF curve of the simulated rain series fall approximately within the confidence limits of both locations for these two return periods. However, the findings by Paludan *et al.* (2014) indicate that the deviation between the statistical properties of the historical SVK series and the synthetic series generates more fundamental problems for the application of the synthetic series where historical series presently are applied. As reviewed in Section 4.7 daily, monthly, and annual properties seem to be fine, which indicates that the weather generator works as anticipated. However, the disaggregation to finer temporal resolution seems to have too high probability of shifting between dry and wet weather. This leads to unreasonable weather patterns.

The programming of the weather generator and the disaggregator has been developed and verified on several data sets, which should exclude programming errors. The methods have been shown to work sufficiently well on several other locations in similar climates, so it should work. The most likely cause is that the weather generator on present climate is calibrated on Climate Grid Denmark while the disaggregator is calibrated on SVK data. Differences in the properties of daily data between these datasets are likely to generate a problem, since the SVK data set uses a high dry weather threshold, which leads to a proportion of dry days considerably larger than Climate Grid Denmark. Another possible cause is that the disaggregation method itself is not performing well. Other formulations of the downscaling cascade allow some form of “memory” between each of the cascades and uses different distribution functions for each cascade.

The series must perform well on the entire range of the IDF-curves of relevance, as well as larger temporal variations on seasonal and annual scale. The fact that the “mean” and “high” climate change impact calculated based on the ENSEMBLES database are combined with other information to yield overall higher estimates of the overall climate change impact further adds to the complexity in the sense that we cannot choose the “standard *CF*” and “high *CF*” synthetic rain series from the simulations directly, but must choose one based on climate factors derived on all methods used in the project. In the current context that means that the “high *CF*” synthetic rain series is very high in the sample of rain series generated by means of this particular approach.

There are no easy solutions to solve this problem. A completely new analysis needs to be done using a different dataset to represent present climate data at high temporal resolution as well as daily data. Two data sets are available:

- SVK data: This has been done in relation to Skrift 29 and can be used again. The main shortcoming of this dataset is that the proportion of dry days is most likely too high and that the mean annual precipitation is underestimated.
- Synop-stations: This data has now been collected for several years with 15 minute resolution and may be suitable. To the best of our knowledge no assessment of the Danish data has been carried out yet.

Hence it must be concluded that the present project has not been able to construct suitable synthetic rain series in high temporal resolution that perform so well that we can recommend them for analysis and design of urban drainage systems.

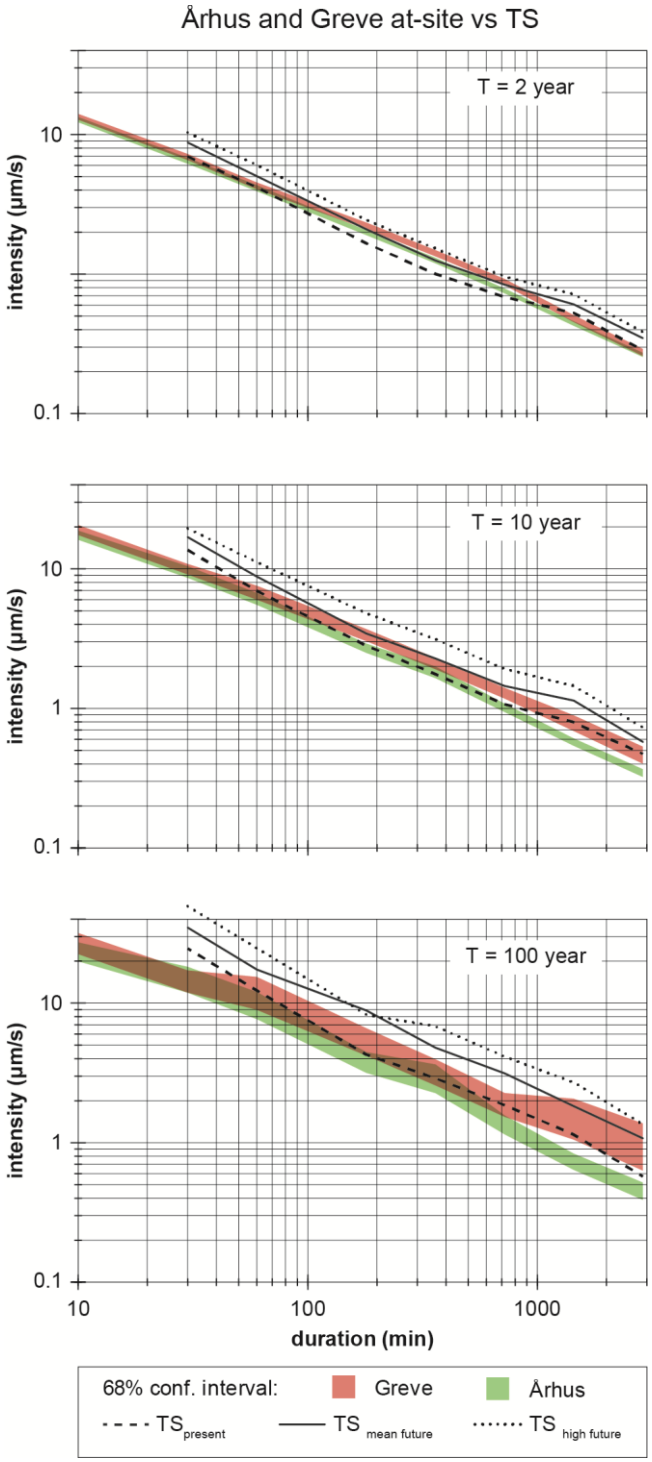

Figure 38: Comparison between the simulated time series representing the present (stipulated lines), future with a standard *CF*, future with a high *CF* and at-site information for Greve (red) and Århus (green). A GDP is fitted to the historical series allowing for an estimation of the 68% confidence intervals for the each site. TS denotes time series.

5.4 Effect of the new guidelines for Greve and Århus

This section evaluates the specific effect of the new guidelines, including both the new regional model (Section 4.1) and the two set of *CF*s (Section 4.5), for the municipalities of Greve and Århus. The use of the synthetic rainfall series are discarded as discussed in Section 5.3.

The geographical location of Greve and Århus is represented by the two main rain gauges of each municipality:

- **Greve:** Mosede waste water treatment plant, station no. 30451, 706565E 6163375N, MAP of 604 mm/year
- **Århus:** Viby J. waste water treatment plant, station no. 22361, 571099E 6220681N, MAP of 665 mm/year

The effect of the guidelines for Greve and Århus is given in Table 10 and Table 11, respectively. It is seen that the effect of the new regional model in itself is minor (below 7%), while it in combination with the new high scenario climate factors leads to an increase of more than 100% for the 100-year event. The relative effect of the new guidelines is similar for the two locations, as expected from Section 5.2.

Table 10: Effect of new guidelines for Greve. Estimated T year events in µm/s precipitation duration 10 min. Relative change in comparison to SVK28 is given in parenthesis.

	2-year event	10-year event	100-year event
Guideline no. 28	12.74	19.51	31.69
Guideline no. 28 + 29	15.29 (20%)	25.37 (30%)	44.36 (40%)
New regional model	13.69 (7%)	20.95 (7%)	34.17 (7%)
New regional model +CF_{mean}	16.43 (29%)	27.24 (40%)	47.84 (51%)
New regional model +CF_{high}	19.85 (56%)	35.62 (83%)	68.34 (116%)

Table 11: Effect of new guidelines for Århus. Estimated T year events in µm/s. precipitation duration 10 min. Relative change in comparison to SVK28 is given in parenthesis.

	2-year event	10-year event	100-year event
Guideline no. 28	13.10	19.95	32.25
Guideline no. 28 + 29	15.72 (20%)	25.93 (30%)	45.16 (40%)
New regional model	13.97 (7%)	21.29 (7%)	34.62 (7%)
New regional model +CF_{mean}	16.76 (28%)	27.68 (39%)	48.47 (50%)
New regional model +CF_{high}	20.26 (55%)	36.19 (81%)	69.24 (115%)

The two case study areas are not alike. Århus is a large city with a large catchment area and a varied terrain with a downwards slope towards the centre of the city. Greve is a small city with a very flat terrain. To compare the change in flood risk using the new guidelines the percentage of flooded city area is estimated for both case study areas. An area is assumed flooded when the water level on the terrain reaches 10 cm or more. Not all combinations of regional models (guideline no. 28 or new regional model) and climate factors (no factor, mean or high) have been tested in the simulations. The results are given in Table 12 and Table 13. For details on the model setup for the two cities see Paludan *et al.* (2014)

Table 12: Flooded city area in Greve [%], the total city area is 1750 ha. The relative change between an application of guideline no. 28 + 29 versus the new regional model + high *CF* is given in parenthesis.

	10-year event	100-year event
Guideline no. 28 + 29	2.6%	6.5%
New regional model + CF_{high}	4.4% (+68%)	11.2% (+73%)

Table 13: Flooded city area in central Århus [%], the total city area is 2000 ha. The relative change between an application of guideline no. 28 + 29 versus the new regional model + high *CF* is given in parenthesis.

	10-year event	100-year event
Guideline no. 28 + 29	0.9%	5.5%
New regional model + CF_{high}	2.2% (+138%)	11.6% (+110%)

6. Conclusion

In relation to the three project objectives in can be concluded that:

1) Analyses of the data from the SVK rain gauge network found that the number of extreme events and the mean intensity of the extreme events have increased during the 34 years of observation. The fact that there is a significant increase cannot be interpreted as a sign of climate change, but must be assessed and attributed to natural climate variation and dynamics as well as climate change caused by anthropogenic emissions of GHG. Analysis of long historical precipitation series shows that both natural climate variation (seen as multidecadal variations expressed as a fluctuation between periods with a relatively high and a relatively low number of extremes in smoothed series of observations) and natural climate change (seen as a general increase) plays a very important role. It is at present not clear how big a proportion of the increase over the last century that can be attributed to human emissions, but it is very likely that the increase observed over the last 30 years is dominated by natural variability.

   An improved model for regional variation of extreme rainfall has been made. The improvements arise from an extended period of measurements (1979-2012) and a new explanatory variable for the regional variation of the mean intensity of the extreme events. The latter being regional information on the mean intensity of daily extreme precipitation from Climate Grid Denmark made by DMI. The resulting change in recommended design intensity in comparison to guideline no. 28 varies both with the duration, return period and location in Denmark. For a 2-year event the change ranges from -9% to 26%.

2) Climate factors that reflect the uncertainty on the future design intensities were estimated, taking both climate model uncertainty, variation over Denmark, the uncertainty of the future climate forcing scenario and the uncertainty of the applied downscaling method into account. On this basis standard climate factor of 1.2, 1.3 and 1.4 are recommended for a 2- , 10- and 100-year event, respectively, as the best estimate of the expected future changes. Additionally, high climate factors of 1.45, 1.7 and 2.0 are recommended for a 2- , 10- and 100-year event, respectively, as an estimate of the upper 84%-quantile of the expected future changes. It should be noted that the natural variation discussed above can lead to a variation in design values that are comparable to the expected effect of climate change (expressed by the mean climate factor).

3) Synthetic precipitation series were generated for the present and two future scenarios, represented by the two set of climate factor mentioned above. However, it was found that the series cannot be used in drainage models because sub-daily precipitation is not realistically generated.

List of abbreviations

CA	Climate Analogue
CF	Climate Factor
CGD	Climate Grid Denmark
DC	Delta Change
DMI	Danish Meteorological Institute
GCM	Global Climate Model
GHG	Greenhouse gases
GPD	Generalized Pareto distribution
IDF	Intensity-Duration-Frequency
MAP	Mean annual precipitation
NRM	New regional model
NSRP	Neyman-Scott Rectangular Pulse
PDS	Partial Duration Series
POT	Peak over Threshold
RCM	Regional Climate Model
RCP	Representative Concentration Pathways
RMSE	Root-Mean-Squared-Error
SVK	Regional rain gauge network maintained by WPC
WG	Weather Generator
WMO	World Meteorological Organisation
WPC	Water Pollution Committee of the Society of Danish Engineers

List of symbols

α	the temporal resolution in the disaggregation cascade model
a	regression parameter
b	regression parameter
$C_{extreme}$	selected extreme value characteristic
CF	Climate Factor
ε	regression error
κ	shape parameter in the generalized Pareto distribution
λ	average annual number of extreme events [no./year]
l	location in space for estimation of CF
L_{cv}	L-moment coefficient of variation
μ	mean value of extreme exceedances in the Partial Duration Series [µm/s]
μ_{CGD}	mean value of the daily precipitation extremes of the CGD data [µm/s]
N	annual number of extreme events [no.]
p	statistical probability
pf	perturbation factor
pf_{λ}	perturbation factor for the average annual number of extreme events
pf_{μ}	perturbation factor for mean value
q	the order of non-central moments used in the scaling relationship of the disaggregation cascade model
τ	the inverse slope of the regression lines estimated for the scaling relationship of the disaggregation cascade model
$t + \Delta t$	present time plus the length of the projection period for estimation of CF
t_c	precipitation duration
t_{full}	full series used for the estimation of pf
t_{sub}	sub series used for the estimation of pf

t_y	time in years since 1979
z_0	location parameter in the generalized Pareto distribution and threshold in the Peak over Threshold approach
z_T	T-year event

References

Arnbjerg-Nielsen, K. (2012). Quantification of climate change effects on extreme precipitation used for high resolution hydrologic design. *Urban Water Journal*. 9(2), 57-65.

Arnbjerg-Nielsen, K., Funder, S.G. and Madsen, H. (in prep.). EurAnalogue: A software tool to identify climate analogues within Europe based on RCM simulations

Arnbjerg-Nielsen, K., Leonardsen, L. and Madsen, H. (submitted). Identifying climate change adaptation options for pluvial flooding based on high-end emission scenarios. *Climate Research*

Burton, A., Fowler, H.J., Blenkinsop, S., Kilsby, C.G. (2010). Downscaling transient climate change using a Neyman–Scott Rectangular Pulses stochastic rainfall model. *Journal of Hydrology*. 381(1-2), 18-32.

Burton, A., Kilsby, C.G., Fowler, H.J., Cowpertwait, P.S.P., O'Connell, P.E. (2008). RainSim: A spatial–temporal stochastic rainfall modelling system. *Environmental Modelling & Software.* 23(12), 1356-1369.

Christensen, J. and Christensen, O.B. (2007). A summary of the PRUDENCE model projections of changes in European climate by the end of this century. *Climatic Change*. 81(1 supplement), 7-30.

Christensen, O.B., Drews, M., Christensen, J.H., Dethloff, K., Ketelsen, K., Hebestadt, I. and Rinke, A. (2007). "The HIRHAM Regional Climate Model, version 5(b)." Technical report 06-17. Danish Meteorological Institute.

Christensen, O.B, Yang, S., Boberg, F., Fox Maule, C., Olsen, M., Drews, M., Sørup, H.J.D. and Christensen. J.H (submitted). Europe in a 6 degrees warmer climate, *Climate Research*

Coles, S. (2001). "An introduction to statistical modeling of extreme values". Springer. London, UK.

Cowpertwait, P.S.P. (1998). A Poisson-cluster model of rainfall : high-order moments and extreme values. *Procedings R. Soc. A.* 454(1971), 885-898.

Cowpertwait, P.S.P., O'Connell, P.E., Metcalfe, A.V., Mawdsley, J.A. (1996). Stochastic point process modelling of rainfall . 1 . Single-site fitting and validation. *Journal of Hydrology.* 175(1-4), 17-46.

Gregersen, I. B., Madsen, H., Rosbjerg, D. and Arnbjerg-Nielsen, K. (submitted a). Long term variations of extreme precipitation in Denmark and Southern Sweden. *Climate Dynamics*

Gregersen, I. B., Madsen, H., Willems P. and Arnbjerg-Nielsen, K. (submitted b). Implications of long term oscillations in precipitation extremes on urban drainage design practices. Proc. of ICUD13 Sarawak, Malaysia

Gregersen, I. B., Sørup, H. J. D., Madsen, H., Rosbjerg, D., Mikkelsen, P. S., and Arnbjerg-Nielsen, K. (2013). Assessing future climatic changes of precipitation extremes at small spatio-temporal scales. *Climatic Change*. 118(3-4), 783-797.

Hazeleger, W., Wang, X., Severijns, C., Stefanescu, S., Bintanja, R., Sterl, A., Wyser, K., Semmler, T., Yang, S., van den Hurk, B., van Noije, T., van der Linden, E., and van der Wiel, K. (2012). EC-Earth V2.2:

description and validation of a new seamless earth system prediction model. *Climate Dynamics*. 39(11), 2611-2629.

Hosking, J. R. M. and Wallis, J. R. (1993). Some Statistics Useful in Regional Frequency-Analysis. *Water Resources Research*. 29(2), 271-281.

IPCC. (2000). "Special Report Emission Scenarios." Intergovernmental Panel on Climate Change. Cambridge University Press. Cambridge, UK.

Kilsby, C.G., Jones, P.D., Burton, A., Ford, A.C., Fowler, H.J., Harpham, C., James, P., Smith, A., Wilby, R.L. (2007). A daily weather generator for use in climate change studies. *Environmental Modelling & Software.* 22(12), 1705-1719.

Larsen, A. N., Gregersen, I. B., Christensen, O. B., Linde, J. J., and Mikkelsen, P. S. (2009). Potential future increase in extreme one-hour precipitation events over Europe due to climate change. *Water Science and Technology*. 60(9), 2205-2216.

Lee, T. and Ouarda, T. (2010). Long-term prediction of precipitation and hydrologic extremes with nonstationary oscillation processes. *Journal of Geophysical Research-Atmospheres*. 115(D13107).

Lundholm S.C. and Cappelen J. (2010). "Ekstremnedbør i Danmark 1961-2010 - leverance til Koordineringsenhed for Forskning i klimaTilpasning (KFT)." Technical report tr17-10. Danish Meteorological Institute.

Madsen, H. (1998). "Ekstremregn i Danmark - Statistisk bearbejdning af nedbørsdata fra Spildevandskomiteens regnmåler system 1979-96." Institut for Strømningsmekanik og Vandressourcer, Institut for Miljøteknologi, Danmarks Tekniske Universitet.

Madsen, H., Arnbjerg-Nielsen, K., and Mikkelsen, P. S. (2009). Update of regional intensity-duration-frequency curves in Denmark: Tendency towards increased storm intensities. *Atmospheric Research*. 92(3), 343-349.

Madsen, H., Gregersen, I.B., Arnbjerg-Nielsen, K., (in prep.) Regional frequency analysis of short duration rainfall extremes in Denmark from 1979-2012

Madsen, H., Mikkelsen, P. S., Rosbjerg, D., and Harremoes, P. (2002). Regional estimation of precipitation intensity-duration-frequency curves using generalized least squares regression of partial duration series statistics. *Water Resources Research*. 38(11).

Madsen, H. and Rosbjerg, D. (1997). The partial duration series method in regional index-flood modeling. *Water Resources Research*. 33(4), 737-746.

Mayer S., Maule C.F., Sobolowski S., Christensen O.B., Sørup H.J.D., Sunyer M.A., Arnbjerg-Nielsen K., Barstad I. (submitted). Added value from high-resolution mini-ensemble climate simulations over Scandinavia. *Tellus A*

Molnar, P., Burlando, P. (2005). Preservation of rainfall properties in stochastic disaggregation by a simple random cascade model. *Atmospheric Research.* 77(1-4), 137-151.

Moss, R. H., Edmonds, J. A., Hibbard, K. A., Manning, M. R., Rose, S. K., van Vuuren, D. P., Carter, T. R., Emori, S., Kainuma, M., Kram, T., Meehl, G. A., Mitchell, J. F. B., Nakicenovic, N., Riahi, K., Smith, S. J., Stouffer, R. J., Thomson, A. M., Weyant, J. P., and Wilbanks, T. J. (2010). The next generation of scenarios for climate change research and assessment. *Nature*. 463(7282), 747-756.

Ntegeka, V. and Willems, P. (2008). Trends and multidecadal oscillations in rainfall extremes, based on a more than 100-year time series of 10 min rainfall intensities at Uccle, Belgium. *Water Resources Research*. **44**(7).

Olsson, J. (1998). Evaluation of a scaling cascade model for temporal rainfall disaggregation. *Hydrology and Earth System Sciences*. 2(1), 19-30.

Paludan B. and Andersen, H. S. (2014). “Notat – Fremtidens Regn, Case Studies”. Report from the VTUF project “Rainfall in a future climate”. In Danish only.

Peters G.P., Andrew R.B., Boden T., Canadell J.G., Ciais P., Le Quéré C., Marland G., Raupach M.R., Wilson C. (2013). The challenge to keep global warming below 2 °C. *Nature Climate Change*, 3, 4–6.

Refsgaard, J., Madsen, H., Andreassian, V., Arnbjerg-Nielsen, K., Davidson, T., Drews, M., Hamilton, D., Jeppesen, E., Kjellstrom, E., Olesen, J., Sonnenborg, T., Trolle, D., Willems, P., and Christensen, J. (2014). A framework for testing the ability of models to project climate change and its impacts. *Climatic Change*. 122(1-2), 271-282.

Rosbjerg, D., Madsen, H., and Rasmussen, P. F. (1992). Prediction in Partial Duration Series with Generalized Paretodistributed Exceedances. *Water Resources Research*. 28(11), 3001-3010.

Scharling,M. (2012). "Climate Grid Denmark - Dataset of use in research and education - Daily and monthly values 1989-2010." Technical report 12-10. Danish Meteorological Institute, Ministry of Climate and Energy. Copenhagen, Denmark.

Scharling,M. and Kern-Hansen,C. (2000). "Klimagrid Danmark - Praktisk anvendelse af nedbørskorrektion på gridværdier." Technical report 00-21. Danish Meteorological Institute, Ministry of Climate and Energy. Copenhagen, Denmark.

WPC (1950). “ Bearbejdelse af diagrammer fra de af Stads- og Havneingeniørforeningen opstillede selvregistrerende regnmålere for årene 1933-47, skrift nr. 2”, The Water Pollution Committee of the Society of Danish Engineers. Available online (downloaded May 2014): http://ida.dk/sites/prod.ida.dk/files/02Diagrammerfrastadsoghavneingeniørforeningen.pdf

WPC (1953). “Bestemmelse af regnrækker, skrift nr. 6”, The Water Pollution Committee of the Society of Danish Engineers . Available online (downloaded May 2014): http://ida.dk/sites/prod.ida.dk/files/06Bestemmelseafregnrækker.pdf

WPC (1974). “Bestemmelse af regnrækker, skrift nr. 16”, The Water Pollution Committee of the Society of Danish Engineers. Available online (downloaded May 2014): http://ida.dk/sites/prod.ida.dk/files/16Bestemmelseafregnrækker.pdf

WPC (1999). “Regional variation af ekstremregn i Danmark, skrift nr. 26”, The Water Pollution Committee of the Society of Danish Engineers. Available online (downloaded May 2014): http://ida.dk/sites/prod.ida.dk/files/26RegionalvariationafekstremregniDanmark.pdf

WPC (2005). “Funktionspraksis for afløbssystemer under regn, skrift nr. 27”, The Water Pollution Committee of the Society of Danish Engineers. Available online (downloaded May 2014): http://ida.dk/sites/prod.ida.dk/files/Skrift27Funktionspraksisforafløbssystemerunderregn.pdf

WPC (2006). “Regional variation af ekstremregn i Danmark – ny bearbejdning 1979-2005, skrift nr. 28”, The Water Pollution Committee of the Society of Danish Engineers. Available online (downloaded May 2014): http://ida.dk/sites/prod.ida.dk/files/SVKskriftnr28.pdf

WPC (2008). “Forventede ændringer i ekstremregn som følge af klimaændringer, skrift nr. 29”, The Water Pollution Committee of the Society of Danish Engineers. Available online (downloaded May 2014): http://ida.dk/sites/prod.ida.dk/files/SVK_Skrift29_final.pdf

Sunyer, M. A., Gregersen, I. B., Madsen, H., Luchner, J., Rosbjerg, D., and Arnbjerg-Nielsen, K. (in review a). Comparison of different statistical downscaling methods to estimate changes in hourly extreme precipitation using RCM projections from ENSEMBLES. *International Journal of Climatology*

Sunyer, M. A., Gregersen, I. B., Madsen, H., Rosbjerg, D., and Arnbjerg-Nielsen, K. (submitted). Extreme precipitation in a future climate – assessing climate factors at sub-daily scales from Regional Climate Model projections. Proc. of ICUD13, Sarawak, Malaysia

Sunyer, M.A., Madsen, H., Ang, P.H. (2012). A comparison of different regional climate models and statistical downscaling methods for extreme rainfall estimation under climate change. *Atmospheric Research.* 103(), 119-128

Sunyer M.A., Madsen H., Rosbjerg D., Arnbjerg-Nielsen K. (in review b). A Bayesian approach for uncertainty quantification of extreme precipitation projections including climate model interdependency and non-stationary bias. *Journal of Climate*

Sunyer, M. A., Sørup, H. J. D., Christensen, O. B., Madsen, H., Rosbjerg, D., Mikkelsen, P. S., and Arnbjerg-Nielsen, K. (2013). On the importance of observational data properties when assessing regional climate model performance of extreme precipitation. *Hydrology and Earth System Sciences*. 17(11), 4323-4337.

Sørup, H.J.D., Christensen, O.B., Arnbjerg-Nielsen, K. and Mikkelsen P.S. (in prep.) Downscaling future precipitation extremes to urban scales using a spatio-temporal Neyman-Scott model. *Climatic Change*.

van der Linden,P., Mitchell,J.F.B. and (Eds). (2009). "ENSEMBLES: Climate Change and its Impacts: Summary of research and results from the ENSEMBLES project." Met Office Hadley Center. Exeter, UK.

van Vuuren, D. P., Edmonds, J., Kainuma, M., Riahi, K., Thomson, A., Hibbard, K., Hurtt, G. C., Kram, T., Krey, V., Lamarque, J. F., Masui, T., Meinshausen, M., Nakicenovic, N., Smith, S. J., and Rose, S. K. (2011). The representative concentration pathways: an overview. *Climatic Change*. 109(1-2), 5-31.

Westra, S., Alexander, L. V., Alexander, L. V., and Zwiers, F. W. (2013). Global increasing trends in annual maximum daily precipitation. *Journal of Climate*. **26**(11), 3904-3918.

Willems, P. (2013a). Multidecadal oscillatory behaviour of rainfall extremes in Europe. *Climatic Change*. 120(4), 931-944.

Willems, P. (2013b). Personal communication, May 2013.

Willems,P., Olsson,J., Arnbjerg-Nielsen,K., Beecham,S., Pathirana,A., Gregersen,I.B., Madsen,H., and Nguyen,V.T.V. (2012). "Impacts of Climate Change on Precipitation Extremes and Urban Drainage Systems". IWA Publishing Compan

Appendix 1 - SVK stations

Station	Name	Easting	Northing	Observation period [years]
20097	Frederikshavn Materielgård	589564	6368352	20.02
20099	Frederikshavn Centralrenseanlæg	591625	6365840	21.02
20211	Sulsted	557766	6336906	30.08
20212	Vodskov	562047	6328974	12.38
20298	Gistrup	560707	6317424	13.07
20304	Aalborg Østerport Pumpestation	557584	6322923	22.69
20307	Aalborg Renseanlæg Vest	552479	6323093	14.76
20309	Nørresundby Søvangen Pumpestation	555264	6324523	14.77
20456	Frejlev Syd Lannerparken	549416	6317777	15.11
20458	Frejlev Nord Verdisvej	549809	6318783	15.21
20461	Svenstrup J.	550779	6315043	24.87
21192	Skive Renseanlæg	502699	6268933	12.14
21207	Skive Lufthavn	510142	6267743	13.00
22123	Grenaå Ådalen P40	617298	6253558	15.72
22321	Egå Renseanlæg	577191	6230496	22.57
22361	Viby J. Renseanlæg	571099	6220681	31.94
22421	Silkeborg Vandværk	534704	6224068	32.99
22554	Trankær Renseanlæg	570631	6215761	23.20
23127	Horsens Centralrenseanlæg	553589	6190188	29.83
23261	Vejle Centralrenseanlæg	533875	6173068	28.85
23294	Fredericia Centralrenseanlæg	545527	6156434	17.98
23321	Kolding Forrenseanlæg	530709	6149146	32.77
23345	Vamdrup Flyveplads	521130	6143760	12.00
24292	Herning Centralrenseanlæg	496400	6222388	32.06
25171	Esbjerg Renseanlæg V	463950	6149223	31.51
26091	Haderslev Renseanlæg	532139	6122624	30.96
26376	Tønder Centralrenseanlæg	490655	6086069	18.65
26481	Sønderborg Damgade Pumpestation	551486	6086668	32.74
28181	Bolbro Højdebeholder	584149	6139144	31.15
28182	Dalum Vandværk	587103	6135399	15.76
28183	Ejby Mølle Renseanlæg	589914	6140044	21.61
28184	Odense NV Renseanlæg	586479	6142454	31.21
28186	Odense Vandværk	586881	6139403	30.98
28453	Svendborg Centralrenseanlæg	607489	6102984	17.97
28461	Svendborg Vandværksvej	601534	6102919	10.69
28503	Ærøskøbing Renseanlæg	590677	6082688	10.01
29009	Gniben	642058	6209353	11.89
29041	Holbæk Centralrenseanlæg	671258	6178244	33.32
29122	Sønder Nyrup Renseanlæg	628775	6173741	11.22
29142	Kalundborg Renseanlæg	632349	6170979	11.25
29354	Slagelse Centralrenseanlæg	648247	6143701	17.51

29429	Omø Fyr	635959	6114654	9.98
30031	Sydkystens Renseanlæg	721870	6211156	33.32
30131	Frederikssund Centralrenseanlæg	692125	6191484	20.78
30168	Hillerød Centralrenseanlæg	704236	6204686	20.89
30191	Furesø Park	715343	6189623	32.11
30201	Vedbæk Renseanlæg	722835	6194852	32.63
30208	Ordrup Kirkegård	724243	6185794	20.78
30211	Svanemøllens Kaserne	724079	6180448	10.87
30218	Stades Krog Overløbsbassin	719641	6186406	13.85
30221	Virum	718976	6187074	18.36
30222	Søborg Vandværk	721023	6181403	32.69
30242	Stavnsholt Resnseanlæg	713405	6190505	12.17
30309	Åvendingen	717713	6178375	15.75
30311	Emdrup	722776	6180425	15.13
30312	Vølundsgade	723133	6178508	14.51
30313	Kløvermarksvej	726591	6175224	32.72
30314	Kongens Enghave	722323	6172103	32.77
30315	Husum	717514	6179276	14.64
30316	Måløv Renseanlæg	708184	6184284	32.84
30317	Glostrup Genbrugsstation	715026	6174858	32.32
30318	Hvidovre Vandværk	718493	6171690	32.58
30319	Hvidovre Pumpestation	718914	6169041	32.36
30321	Rødovre Vandværk	717736	6177448	33.04
30325	Bispebjerg Hospital	722536	6180239	17.85
30326	Lygten	722328	6178996	17.62
30348	Wibrandtsvej	728571	6172885	17.48
30351	Tårnby Pumpestation 4	726328	6171028	33.17
30352	Tårnby Pumpestation 10	725673	6167768	33.14
30353	Tårnby Renseanlæg	729886	6171908	30.53
30381	Landbohøjskolen	722765	6176850	20.49
30384	Brøndbyvester Vandværk	714900	6171328	21.13
30386	Albertslund Materielgård	710055	6173719	18.96
30388	Høje Tåstrup	704927	6173114	16.89
30395	Ishøj Varmeværk	710957	6167192	20.00
30411	Roskilde Renseanlæg	692386	6171355	32.14
30451	Mosede Renseanlæg	706565	6163375	32.55
31031	Store Heddinge Vandværk	715202	6135001	12.33
31151	Næstved Centralrenseanlæg	673598	6121674	31.27
31231	Vordingborg Renseanlæg	684908	6098964	12.61
31401	Nakskov Renseanlæg	636068	6077346	32.89
31511	Nykøbing F Renseanlæg	685279	6073444	32.43
32097	Rønne C	864080	6121110	22.73

Appendix 2 - Regional model parameters

Table 14: The threshold, zo, the average annual number of extreme events, λ (averaged over all included stations and all years of measurements) and the mean intensity, μ (averaged over all included stations and all years of measurements). The same threshold is applied for the three different regional models. The μ-values marked by italic indicate a different unit.

	z0	λ [year^{-1}]			μ [μm/s]*[mm]*		
		SVK26	SVK28	NRM	SVK26	SVK28	NRM
1 min intensity	15.80	-	3.82	4.28	-	6.02	6.26
2 min intensity	12.80	-	3.80	4.31	-	5.82	6.04
5 min intensity	9.00	-	3.65	4.18	-	4.76	4.93
10 min intensity	6.00	3.22	4.03	4.63	3.34	3.47	3.61
30 min intensity	3.20	3.11	3.79	4.29	1.6	1.73	1.84
60 min intensity	2.10	3.13	3.70	4.12	0.937	1.05	1.13
3 hours intensity	1.10	3.02	3.44	3.69	0.449	0.473	0.519
6 hours intensity	0.73	2.83	3.10	3.35	0.277	0.284	0.316
12 hours intensity	0.45	2.53	2.76	3.09	0.184	0.177	0.194
24 hours intensity	0.26	2.65	2.98	3.25	0.114	0.103	0.110
48 hours intensity	0.15	3.04	3.34	3.52	*0.0684*	*0.0619*	*0.0644*
daily depth	19.40	2.95	3.30	3.47	*8.17*	*8.02*	*8.24*
basin volume 1	17.00	2.82	3.11	3.31	*11*	*10.12*	*10.72*
basin volume 2	5.40	2.85	3.33	3.75	*4.46*	*4.69*	*5.08*

Table 15: The parameters in the regression between λ and MAP (in mm) for the NRM

$\lambda = \hat{b}_0 + \hat{b}_1 \cdot MAP + \varepsilon$	$\hat{b}_0$	$\hat{b}_1$ [x10^{-3}]	$Var(\hat{b}_0)$	$Var(\hat{b}_1)$ [x10^{-6}]	$Cov(\hat{b}_0, \hat{b}_1)$ [x10^{-4}]	σ_ε	R^2
1 min intensity	0.245	6.112	0.763	1.682	-11.06	0.343	0.27
2 min intensity	0.849	5.193	0.831	1.830	-12.03	0.398	0.18
5 min intensity	1.298	4.292	0.832	1.833	-12.05	0.401	0.12
10 min intensity	1.664	4.366	1.060	2.347	-15.41	0.535	0.09
30 min intensity	1.969	3.250	0.903	1.986	-13.07	0.423	0.05
60 min intensity	2.178	2.735	0.908	1.993	-13.13	0.409	0.02
3 hours intensity	1.760	2.720	0.760	1.658	-10.94	0.309	0.03
6 hours intensity	0.873	3.597	0.734	1.588	-10.51	0.306	0.07
12 hours intensity	0.0391	4.415	0.708	1.532	-10.14	0.310	0.13
24 hours intensity	-1.518	7.051	0.688	1.473	-9.77	0.281	0.32
48 hours intensity	-2.741	9.491	0.611	1.293	-8.60	0.213	0.54
daily depth	-1.241	7.037	0.775	1.682	-11.12	0.335	0.28
basin volume 1	-1.039	6.432	0.585	1.259	-8.34	0.214	0.34
basin volume 2	2.449	1.741	0.771	1.701	-11.20	0.328	0

Table 16: The parameters in the regression between μ and μCGD (in mm) for the NRM. The values marked by italic indicate a different unit.

$\mu = \hat{b}_0 + \hat{b}_1 \cdot \mu_{CGD} + \varepsilon$	$\hat{b}_0$	$\hat{b}_1$ [x10^{-2}] *[x10^{0}]*	$Var(\hat{b}_0)$ [x10^{-2}] *[x10^{0}]*	$Var(\hat{b}_1)$ [x10^{-4}] *[x10^{0}]*	$Cov(\hat{b}_0, \hat{b}_1)$ [x10^{-3}] *[x10^{0}]*	σ_ε	R^2
1 min intensity	6.223	0	1.991	0	0	0.221	0
2 min intensity	5.994	0	1.665	0	0	0.128	0
5 min intensity	4.896	0	1.090	0	0	$7.64 \cdot 10^{-2}$	0
10 min intensity	3.577	0	0.622	0	0	$4.42 \cdot 10^{-2}$	0
30 min intensity	1.822	0	0.243	0	0	$2.47 \cdot 10^{-2}$	0
60 min intensity	1.096	0	0.110	0	0	$1.19 \cdot 10^{-2}$	0
3 hours intensity	-0.389	3.332	11.45	1.639	-4.327	$1.22 \cdot 10^{-3}$	0.05
6 hours intensity	-0.443	2.771	4.600	0.657	-1.735	$4.65 \cdot 10^{-4}$	0.13
12 hours intensity	-0.338	1.942	1.371	0.195	-0.516	$4.25 \cdot 10^{-5}$	0.31
24 hours intensity	-0.252	1.353	0.411	0.058	-0.155	$9.28 \cdot 10^{-6}$	0.44
48 hours intensity	-0.0773	0.526	0.148	0.0211	-0.0558	$1.41 \cdot 10^{-5}$	0.13
daily depth	-17.75	*0.9651*	*25.77*	*0.03685*	*-0.973*	0.277	0.35
basin volume 1	-17.00	*1.037*	*53.14*	*0.07586*	*-2.003*	0.530	0.15
basin volume 2	-2.547	*0.2812*	*14.19*	*0.02029*	*-0.536*	0.198	0

Appendix 3 - Trend analysis for all the durations

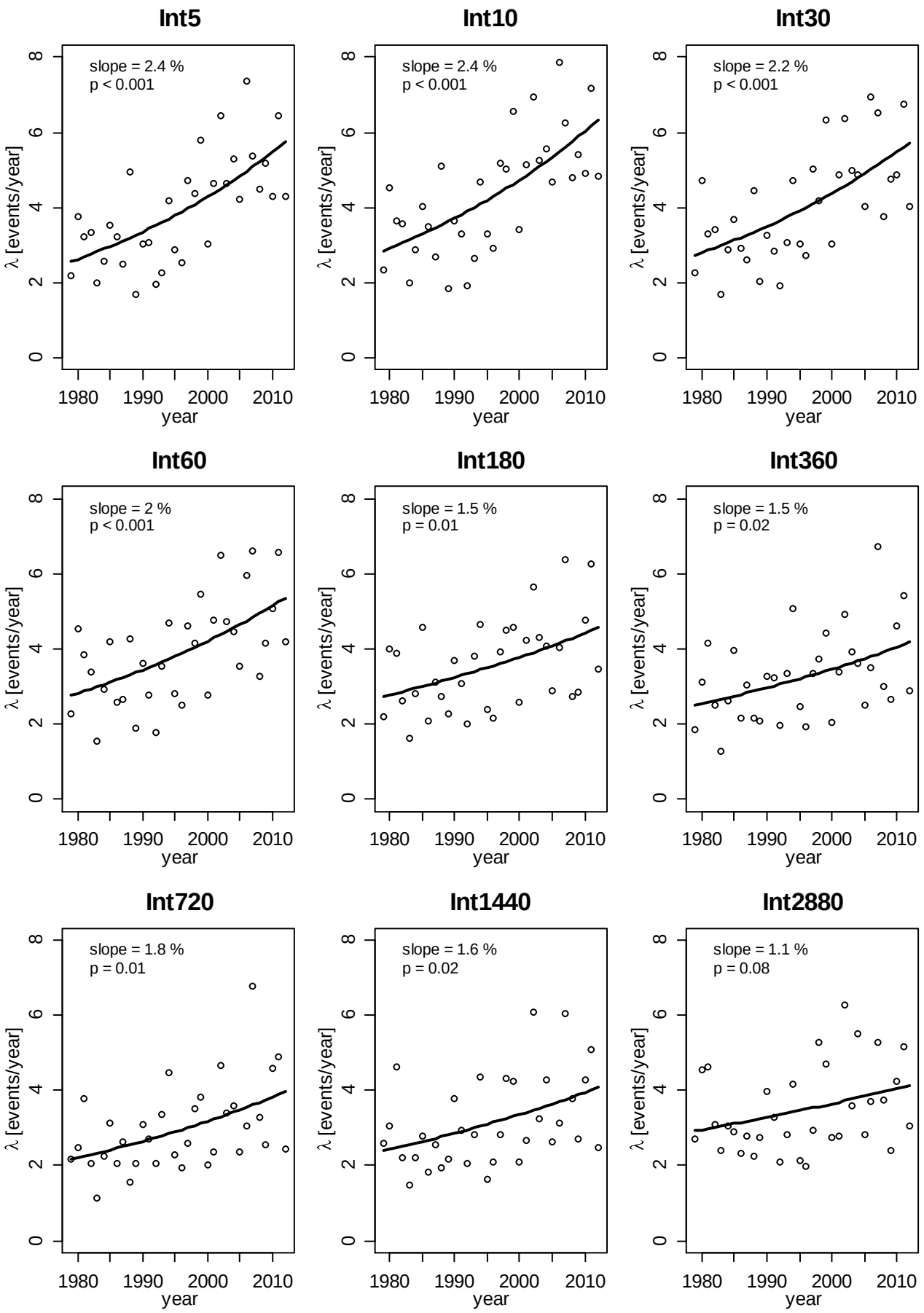

Figure 7: Annual development in the number of extreme precipitation events between 1979 and 2012, evaluated on a regional average of all the SVK stations, for precipitation intensities between 5 min and 2 days. Because Poisson regression is applied the slope is given in percentages. *p* denotes the probability of the estimated slope to being equal to zero, if below 0.05 the increase is significant

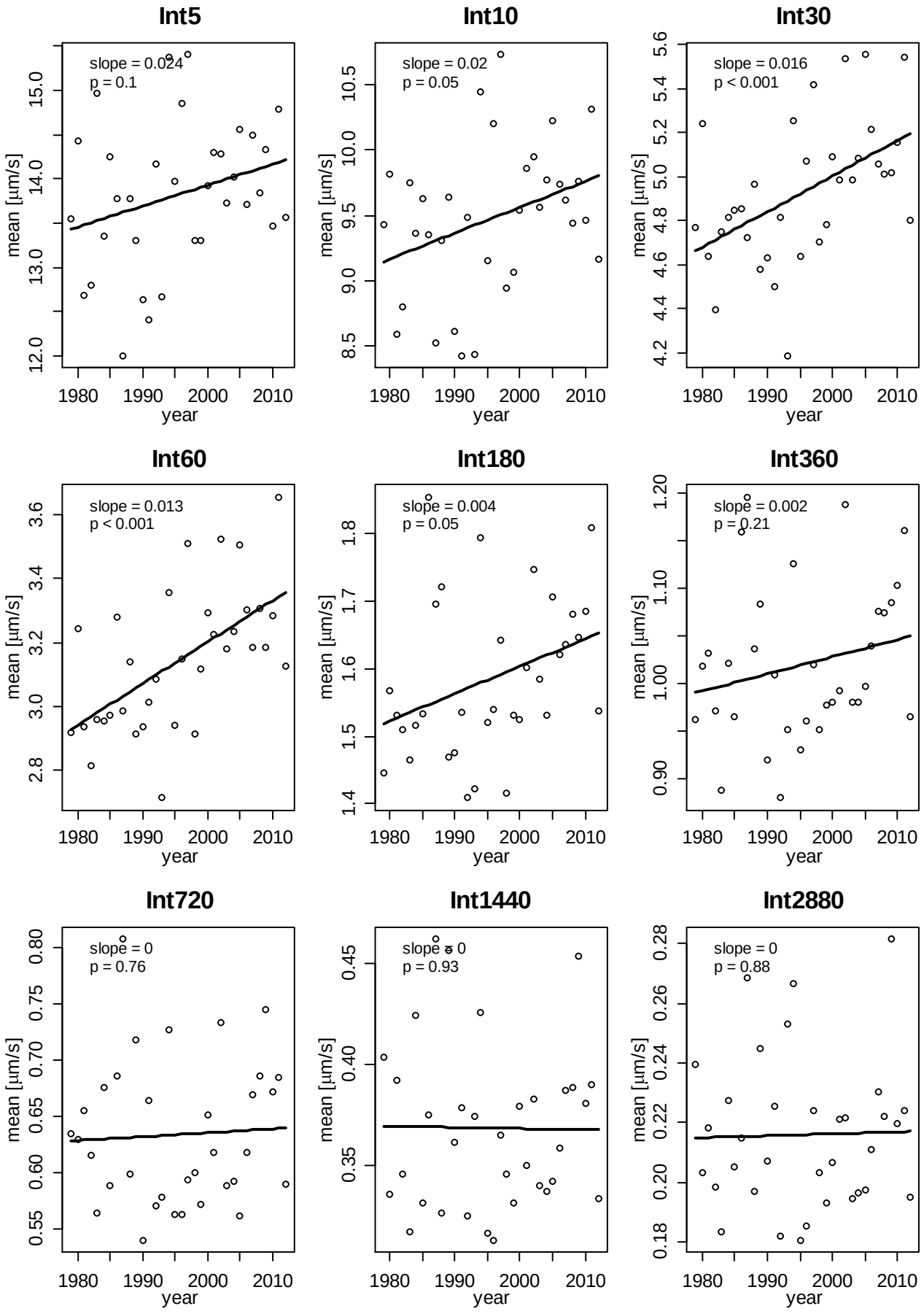

Figure 8: Annual development in the mean intensity of extreme precipitation events between 1979 and 2012, evaluated on a regional average of all the SVK stations, for precipitation intensities between 5 min and 2 days. Because linear regression is applied the unit slope is µm/s/year. *p* denotes the probability of the estimated slope to being equal to zero, if below 0.05 the increase is significant

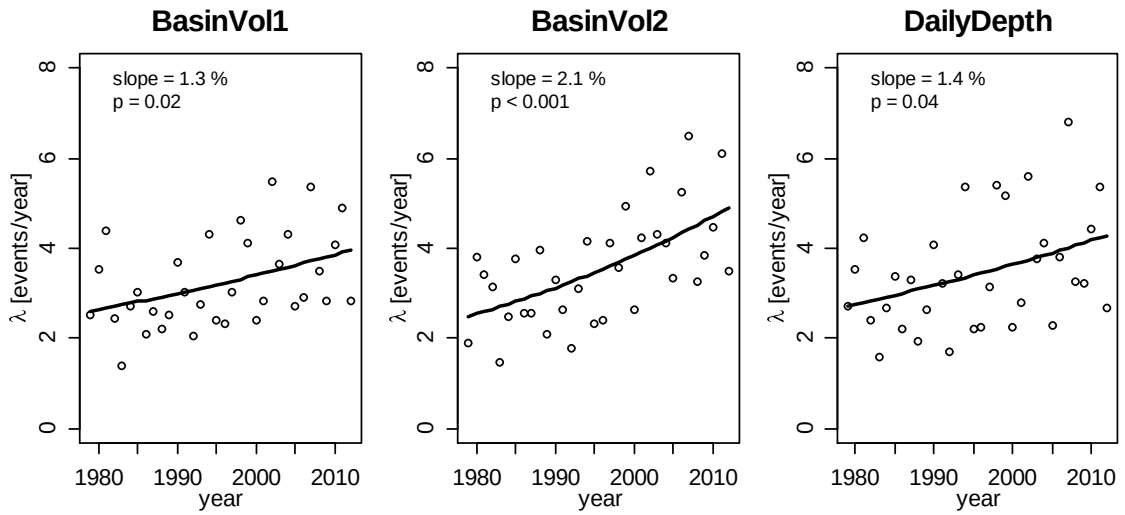

Figure 41: Annual development in the number of extreme precipitation events between 1979 and 2012, evaluated on a regional average of all the SVK stations, for basin volume 1 and 2 and accumulated daily precipitation (for definition see Madsen 1998). Because Poisson regression is applied the slope is given in percentages. p denotes the probability of the estimated slope to being equal to zero, if below 0.05 the increase is significant

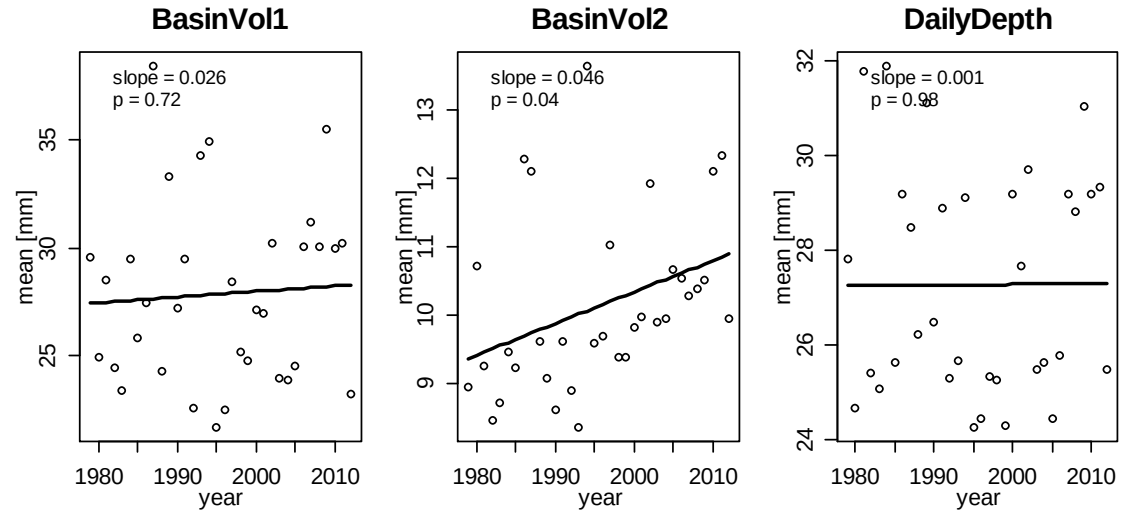

Figure 42: Annual development in the mean intensity of extreme precipitation events between 1979 and 2012, evaluated on a regional average of all the SVK stations, for basin volume 1 and 2 and accumulated daily precipitation(for definition see Madsen 1998). Because linear regression is applied the unit slope is intensity/year. *p* denotes the probability of the estimated slope to being equal to zero, if below 0.05 the increase is significant

Appendix 4 - Oscillations and dependence on the window length

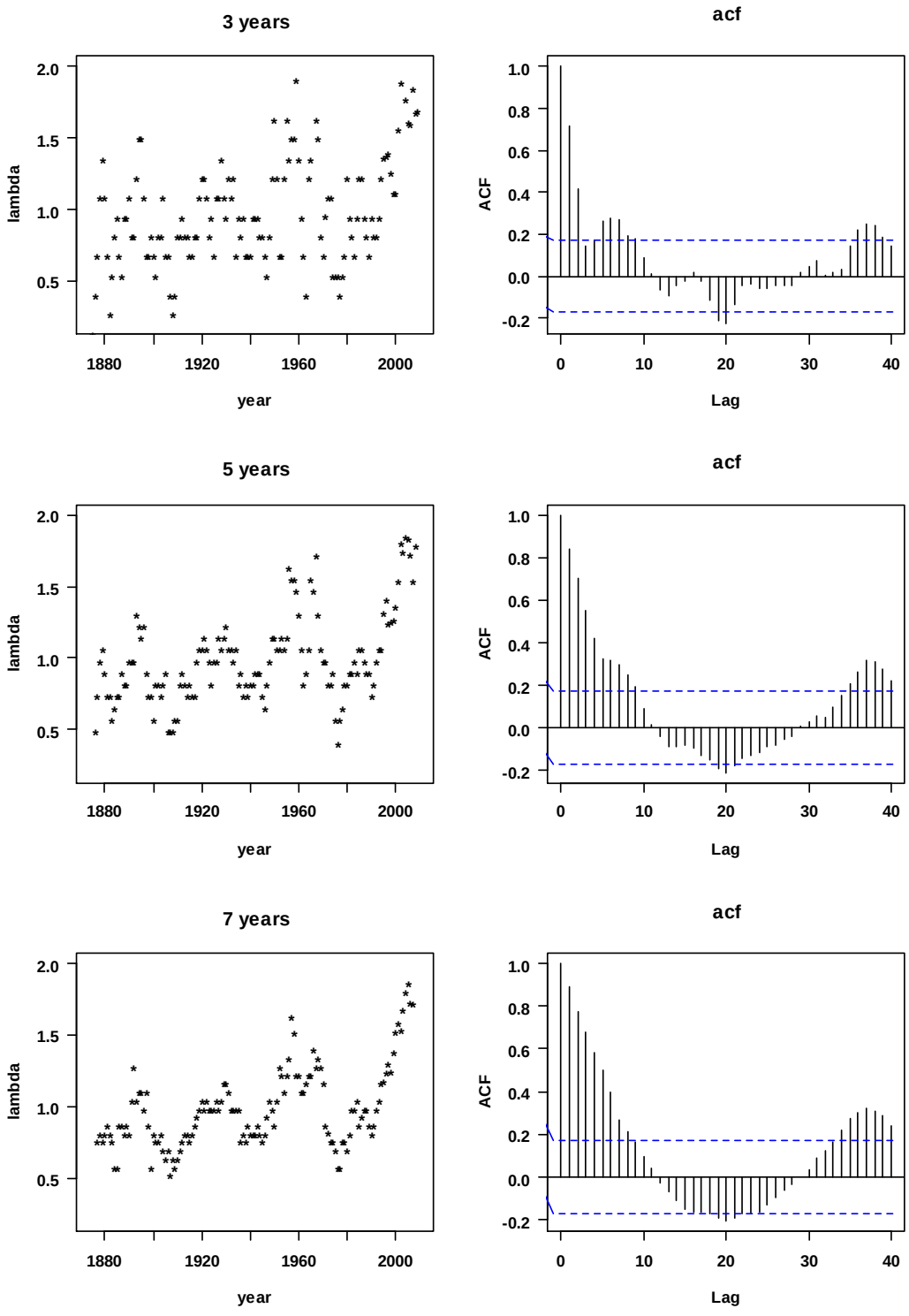

Figure 43: Variation of the oscillation signal with the length of the moving window (3, 5 and 7 years)

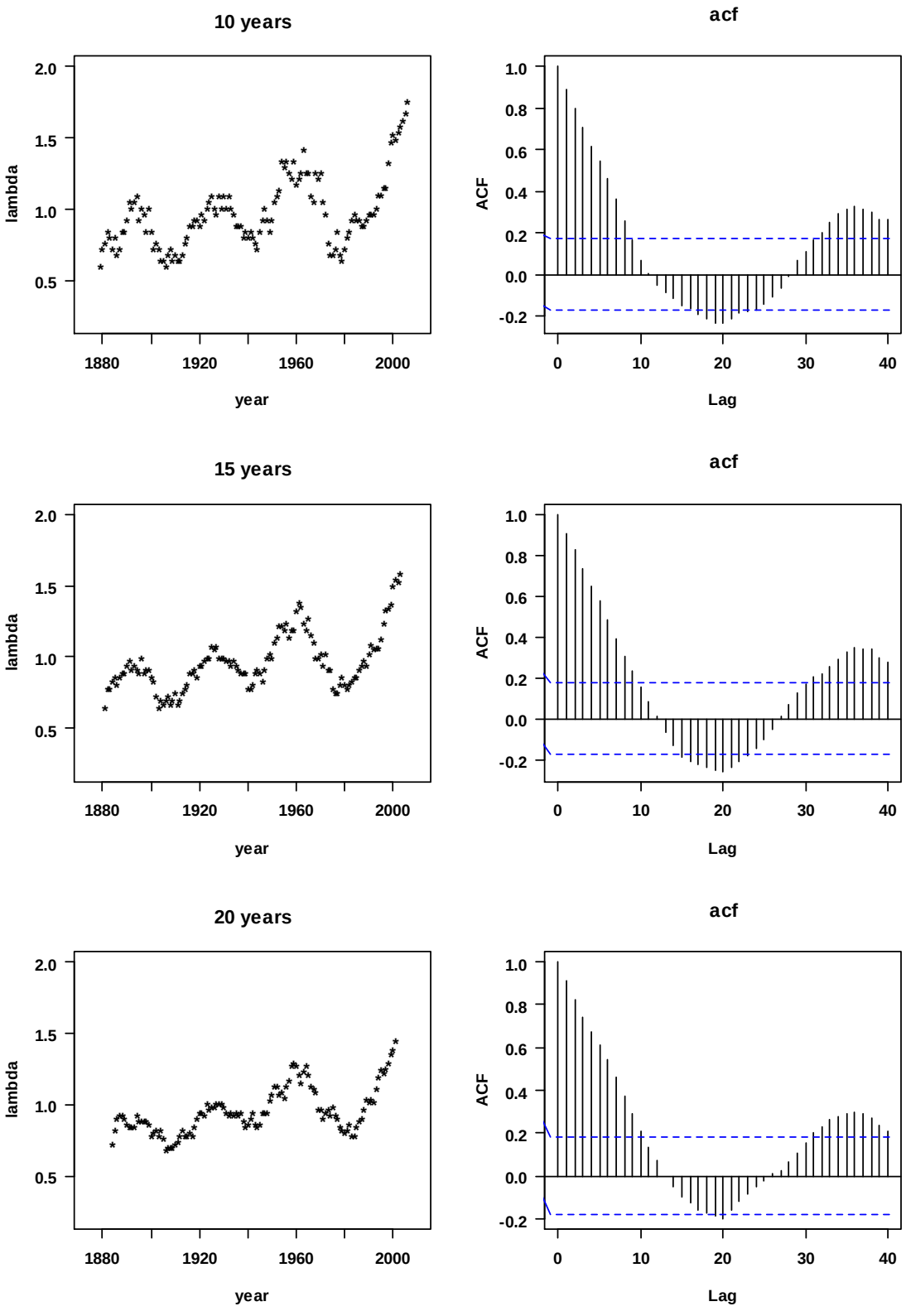

Figure 44: Variation of the oscillation signal with the length of the moving window (10, 15 and 20 years)